Soft-templated mesostructured TiO2 - SiO2 composites with high thermal stability

Bénédicte Lebeau, Florian Jonas, Laure Michelin, Jean-Luc Blin

Soft-templated mesostructured TiO_2 - SiO_2 composites with high thermal stability

Bénédicte Lebeau[1,2*], Florian Jonas[3], Laure Michelin[1,2], Jean-Luc Blin[3]*,

[1]: Université de Haute Alsace (UHA), CNRS, IS2M UMR 7361, F-68100 Mulhouse, France
[2]: Université de Strasbourg, 67000 Strasbourg, France
[3]: Université de Lorraine, CNRS, L2CM, F-54000 Nancy, France

** Corresponding authors: Jean-Luc.Blin@univ-lorraine.fr, Benedicte.Lebeau@uha.fr*

Abstract

To overcome the drawbacks of pure mesostructured titania and in particular the low thermal stability, in this study we have investigated in detail the effect of Si^{4+} addition on the properties of mesostructured TiO_2 prepared by combining the sol-gel process and the surfactant templating mechanism. Obtained materials have also been tested for the photodegradation of methyl orange, used as a model dye.

From the SAXS and the manometry nitrogen adsorption-desorption analyses, it can be concluded that the presence of Si^{4+} delays the collapse of the mesopores network. Compared to the bare mesostructured TiO_2, the XRD and Raman results show that the anatase and the rutile phases appear at higher temperature. The higher the Si^{4+} content, the higher the amorphous-anatase and rutile anatase-phase transition temperatures. The delay in the crystallization also allows the detection of the TiO_2-β phase, which is an anatase phase with oxygen vacancies. These phenomena have been attributed to the « glass effect ». In that case, amorphous SiO_2, which is formed during the synthesis, surrounds the titania particles and inhibits their growth, when the heating temperature is increased. By this way, the thermal stability of the mesostructured titania containing Si^{4+} is enhanced.

Photocatalytic experiments highlight the importance of the presence of the anatase phase for the discoloration efficiency of the dye solution. Indeed, the increase of Si^{4+} leads to a clear decrease of the photodegradation efficiency.

Keywords: Mesostructured Titania; Photo-discoloration, Soft templating, Phase transformation; Glass effect

1. Introduction

Nanomaterials cover a wide range of research fields and applications owing to their exceptional physical and chemical properties. Specially, they play significant roles in catalysis due to features that derive from their high surface to volume ratio. [1] Among them, mesostructured oxides with high specific surface area and well-connected uniform pores are of importance since the access to the active sites is favored [2-4]. Two main pathways can lead to the formation of these mesostructured oxides [5-8]. The first one is the hard-templating method. In that case, the material is prepared in a confined space, for example via replication of mesoporous silica as hard template. Since the template prevents collapse of the mesostructure upon calcination, the main advantage of this method is the preservation of the ordered mesopore channel array during the crystallization step at high temperature. However, this pathway is time consuming (long process), not environmentally friendly, it requires hydrofluoric acid to remove the hard template and can require specific devices and instrumentation. The second way to get the mesostructured oxides is the soft templating pathway, which implies the co-assembly of the inorganic precursor and surfactant (porogen agent), similar to the preparation of ordered mesoporous silica. However, in that case one key parameter that should be considered concerns the control of the precursor hydrolysis and condensation. In fact, precursors such as alkoxides exhibit a high reactivity towards hydrolysis and condensation [9]. Consequently, dense phases with a poor mesopore arrangement and a low specific surface area is often recovered. Among the different non-siliceous oxides, titania is of particular interest. TiO_2 is a semiconductor widely used for applications in electronics, electrochemical systems but also as catalyst, promoter or carrier for metals and their complexes [10-13]. But especially, it is one of the most commonly used oxides for photocatalysis [14-17]. The photocatalytic efficiency depends on several parameters such as the crystal structure, the particle size, the specific surface area and the porosity [18-20]. Indeed, generally, large surface area is likely to exhibit better photocatalytic activity, because a large surface area provides more active sites for adsorption. Thus, up to now, many efforts are still devoted to the synthesis of mesoporous titania with enhanced efficiency [21-25]. For example, using the sol-gel process and starting from titanium isopropoxide as precursor and performing a hydrothermal treatment at different temperatures from 40 to 240°C, Rasalingam *et al.* have synthesized efficient photocatalysts for the degradation of rhodamine B under visible light irradiation [26]. By combining the sol-gel process with the surfactant templating mechanism, reported for the preparation of the ordered mesoporous silica materials in our group, we have developed a synthesis procedure of ordered mesoporous materials, having semi-crystalline framework and with high specific surface area (> 250 m^2/g) [27,28]. These materials are effective catalysts for the photo-degradation of methyl orange [29,30]. The high specific surface area and the semi crystalline framework of the mesostructured TiO_2 are major assets for photocatalysis. However, these compounds have also an important drawback, which is their weak thermal stability. Because of the intrinsic crystallization of anatase [28,31], after being heated at 450 °C, the mesostructure collapses and most of the porosity is lost. Coupling TiO_2 with another oxide appears to be the most common efficient way to enhance the thermal stability of titania [32-36]. For example, Warrier et al. have shown that the addition of 15 mol.% of SiO_2 during the sol gel preparation of TiO_2 allows to maintain a specific surface area of 93 m^2/g after calcination at 800°C [37]. The titania materials modified with SiO_2 exhibit higher efficiency for the photodegradation of methylene blue than the pure TiO_2 sample [37]. In a paper dealing with the synthesis of Zn-TiO_2 oxides by the ball milling method, we have also shown that coupling zinc oxide to mesostructured TiO_2 inhibits the collapse of the structure during calcination, enhancing thermal stability of materials [38]. To overcome the drawback of low thermal stability of mesostructured TiO_2, one solution therefore consists in forming (nano)composites or mixed

oxides by the introduction of heteroelement during the synthesis of titania materials. Here, we have investigated in detail the effect of the Si^{4+}, addition on the properties of soft-templated mesostructured TiO_2 with semi-crystalline framework. A peculiar attention has been paid to the thermal stability and the phase transition temperatures.

2. Materials and methods

The triblock copolymer Pluronic P123 $(EO)_{20}(PO)_{70}(EO)_{20}$ (EO = ethylene oxide, PO = propylene oxide) was purchased from Aldrich. Titanium isopropoxide $Ti(OiPr)_4$, and tetramethylorthosilicate (TMOS) were also purchased from Aldrich and used as inorganic source. Hydrochloric acid (ACS reagent, 37%, Aldrich) and ethanol (99%, Aldrich) were employed to control the rate of hydrolysis of the alkoxides.

2.1. Materials preparation: 1 g of surfactant was first dissolved into 20 g of ethanol under stirring at 300 rpm at room temperature. Then, 2 g of a hydrochloric acid solution (37%), 3 g of titanium isopropoxide [$Ti(OiPr)_4$] were added. Afterwards, x g of TMOS were incorporated. The Si^{4+} content (mol.% compared to Ti^{4+}) in the mixture was varied from 0 to 20 mol.%. After addition of 2g of water, the mixture is directly evaporated under vacuum (55 °C, 25 mbar) to remove ethanol and other alcohols released by hydrolysis of the alkoxides. Samples were dried in an oven at 40°C for 12 h. Then they were placed under an atmosphere of NH_3 (≈ 0.5 atm) for 12 h. For that step, samples were placed during 12 hours in a well-closed glass vessel containing concentrated aqueous ammonia (28 wt.%) in a crystallizer without touching the sample to saturate the atmosphere in gaseous NH_3. The final products were recovered after surfactant extraction with ethanol and Soxhlet during 8 hours. After this step all the materials have an amorphous mesopore framework.
To investigate the effect of Si^{4+} on the thermal stability of the obtained amorphous mesostructured materials, the samples were heated at different temperatures, from 380 to 900°C under air atmosphere in a muffle furnace. To perform this study, they were first heated to 150°C, at a rate of 1 °C / min and kept at this temperature during one hour. Afterwards, the same program was applied to reach the final temperature 380, 500, 600, 700, 800 or 900°C.

2.2. Characterization:
SAXS experiments were performed on a SAXSess mc² instrument (Anton Paar), using a line collimation system. This instrument is attached to a ID 3003 laboratory X-Ray generator (General Electric) equipped with a sealed X-Ray tube (PANalytical, $\lambda_{Cu,\ K\alpha} = 0.1542$ nm) operating at 40 kV and 50 mA. A multilayer mirror and a block collimator provide a monochromatic primary beam. A translucent beam stop allows the measurement of an attenuated primary beam at q=0. Materials were put between two sheets of Kapton® placed in a powder cell before being introduced inside the evacuated chamber. All data were corrected for the background scattering from the Kapton® and for slit-smearing effects by a desmearing procedure from SAXSQuant software using the Lake method. Powder X-ray diffraction patterns were recorded using a PANalytical X'Pert PRO diffractometer equipped with a Cu X-ray tube ($\lambda_{Cu(K\alpha)} = 0.1542$ nm) operating at 45 kV and 40 mA and a X'Celerator detector. Fixed divergence slit (1/16°), mask (10 mm) and antiscatter slit (1/8°) were used at primary beam for the current analysis. The crystallite size was estimated by applying the Scherrer equation using the principal diffraction peak corresponding to the plane (101) of anatase. The Scherrer constant used was $K = 0.9$ and the β instrumental was taken for the FWHM of (101) plane of a micrometric anatase.
N_2 adsorption-desorption isotherms were determined on a Micromeritics TRISTAR 3000 sorptometer at –196 °C. The specific surface area was obtained by using the BET model

whereas the pore diameter and the pore size distribution were determined by the BJH (Barret, Joyner, Halenda) method applied to the adsorption branch [39].
Raman Scattering Spectra were collected on a Jobin-Yvon T64000 spectrometer equipped with an optical microscope in confocal mode. The excitation beam (514.5 nm) was focused using a long-frontal x50 objective (numerical aperture 0.5) on an area of about 3 μm^2. The laser power on the sample was approximately 10 mW. The spectral resolution was 3 cm^{-1}, with a wavenumber precision better than 1 cm^{-1}.
Diffuse reflectance spectra were recorded between 200 and 800 nm at 1 nm increment with an integrated sphere attached to a Cary 5G UV-Vis-NIR spectrophotometer. The relative spectral reflectance R is defined as the ratio between the flux reflected by the sample Rs and that of a PTFE reference Rr. The spectra are shown in pseudo-absorbance (-logR), mode since the use of the Kubelka-Munk function does not improve the quality of the calibration line.

2.1. Photodegradation of methyl orange:
Methyl orange was chosen as organic compound to evaluate the photocatalytic properties of the mesoporous titanates materials. Analyses have been performed according to the procedure we have previously reported [29]. 50 mg of materials have been added to 100 mL of a methyl orange aqueous solution (16 mg per L). The reaction was carried out under continuous stirring in a quartz flask. Samples were irradiated with UV light from a high-mercury lamp. The mean value of the radiation power impinging on the reacting suspension was estimated to be $I_{incident} = 10^{-5}$ Einstein L^{-1} s^{-1}. Prior to UV irradiation, the aqueous TiO_2 suspension containing methyl orange was magnetically stirred in the dark for 1 hour until adsorption/desorption equilibrium was reached. Degradation process of methyl orange was monitored with a Cary 3E UV-Vis-spectrophotometer. The photocatalytic degradation of methyl orange solution was followed by measuring the absorbance value at $\lambda = 464$ nm, which allowed access to the methyl orange concentration. Analytical uncertainty on methyl orange concentration was mainly due to the filtration step and has been evaluated to be 1.5 μg L^{-1}.

3. Results and discussion

3.1 Structural investigation:

Figure 1 depicts the evolution of the SAXS pattern as a function of the heating temperature for the bare TiO_2 and upon the addition of Si^{4+} from 1 to 20 mol.%. The SAXS pattern (of the extracted TiO_2 is characteristic of a mesostructured titania as reported previously [27,28] and upon heating the mesostructure begins to collapse at 600°C. Indeed, after treatment at this temperature a large and not well resolved peak is observed on the SAXS pattern. If the calcination is performed above 600°C, no reflection is detected any longer, reflecting the complete collapse of the mesopore framework. Whatever the Si^{4+} loading, before thermal treatment the SAXS pattern of the extracted TiO_2 is characteristic of mesostructured materials with a broad peak located between 9.2 to 10.6 nm, depending on the Si^{4+} mol.%. After thermal treatment, all the SiO_2-TiO_2 materials present a similar behavior. First, we note a decrease of the d-spacing value because of the network shrinkage upon heating. This phenomenon can be attributed to the condensation of the OH groups and to the probable crystallization of the walls. For example, for mesostructured titania prepared with addition of 5 mol.% of Si^{4+}, the d-spacing varies from 10.0 to 8.3 nm when the heating temperature is raised to 600°C. Secondly, around 700°C a second peak located at higher d values (17.9 nm for 1 mol.% of Si^{4+}) appears. The lower the Si^{4+} content, the more pronounced is this peak. It is characteristic of a correlation distance, which can be related to the presence of crystalline particles. This suggests that the mesostructure collapses, leading to particles with quite homogeneous size. Finally, if the heating temperature is further increased, the correlation distance also increases, meaning that the particles growth, and at the same time the broad

peak, characteristic of the mesostructure disappears. Thus, the mesopore network has completely collapsed. However, the higher the Si^{4+} content, the more this phenomenon is delayed (Table1). For example, after heating at 700°C, no mesostructure can be detected from the SAXS pattern of the TiO_2 containing 1 mol.% of Si^{4+}, whereas the peak at 8.2 nm still reflects the persistence of the mesopore network after heating at 800°C even at 900°C for the titania prepared in the presence of 20 mol.% of Si^{4+} (Fig. 1).

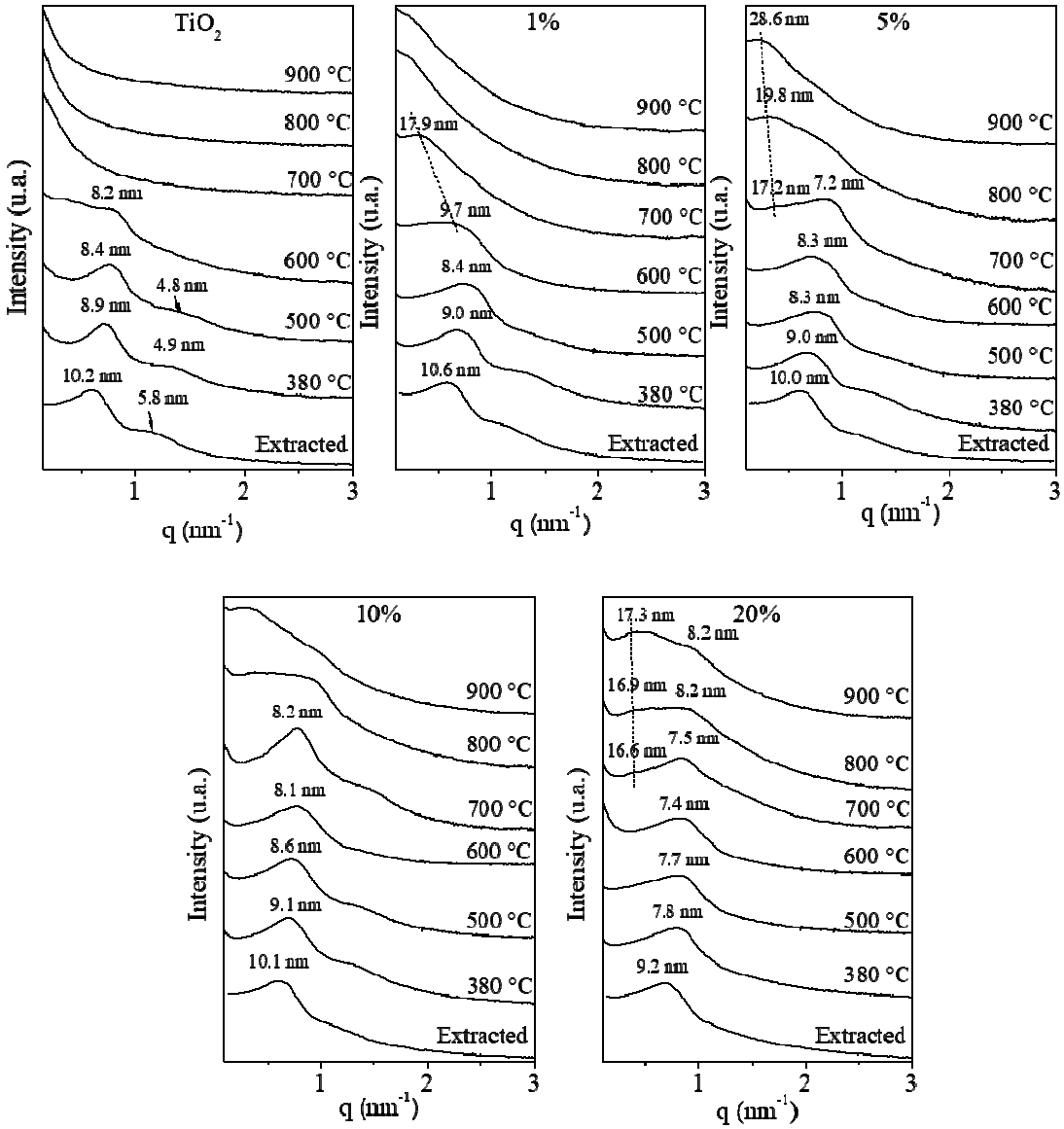

Figure 1: Evolution of the SAXS pattern as a function of the heating temperature of bare TiO_2 and TiO_2 containing 1, 5, 10 or 20 mol.% of Si^{4+}.

Table 1: Collapse temperature (T_C) of the mesostructure, temperature of crystallization into nanosized anatase (T_A), temperature at which the rutile polymorph is detected (T_R) as a function the Si content (mol.%).

Si^{4+} loading (mol.%)	T_C (°C)	T_A (°C)	T_R (°C)
0	600	380	700
1	500	500	800
5	700	500	-
10	700	600	-
20	900	700	-

The crystallization of the walls and the growth of the particles as a function of the heating temperature is further confirmed by the XRD (Fig. 2) analysis.

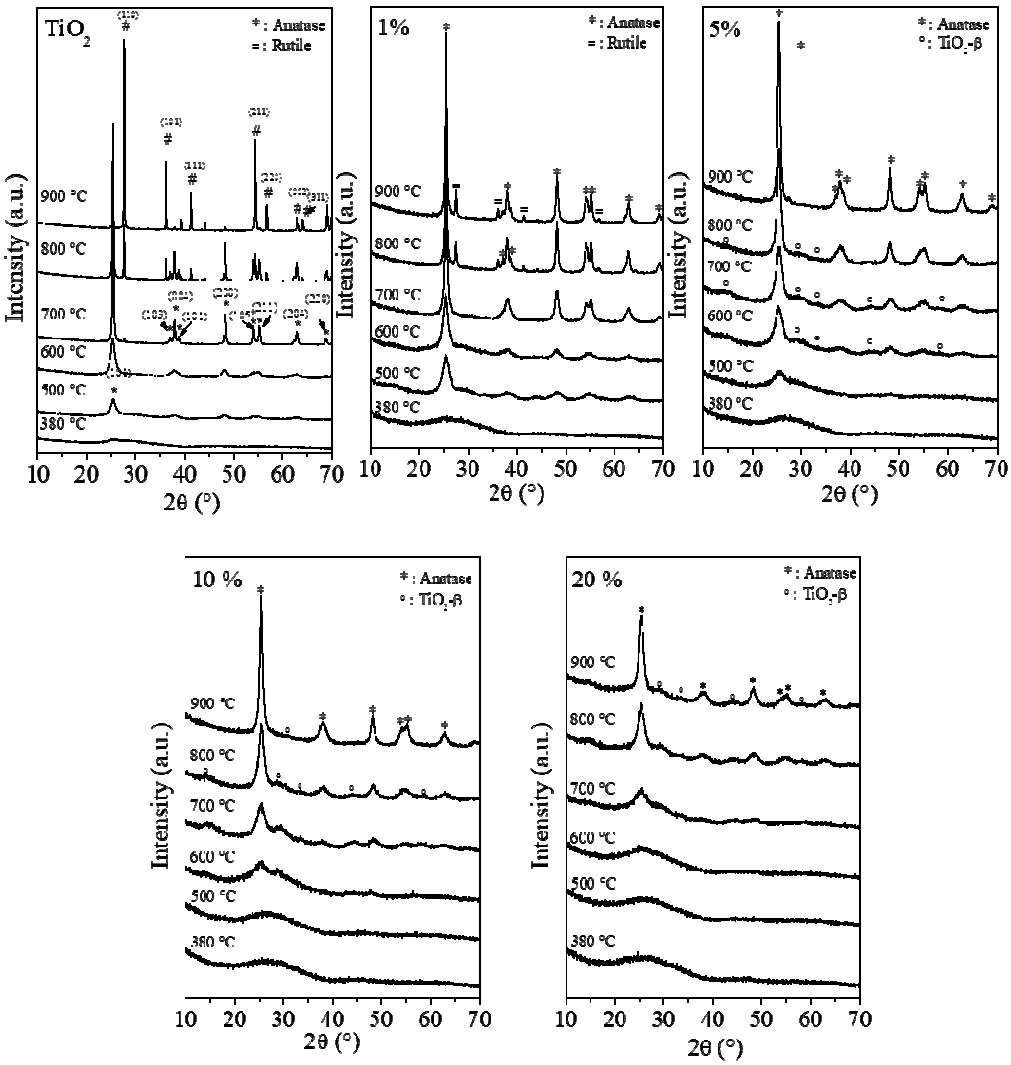

Figure 2: Evolution of the X-Ray diffractogramms as a function of the heating temperature of bare TiO_2 and TiO_2 1, 5, 10 or 20 mol.% of Si^{4+}.

As it can be observed from Figure 2, after heating the bare mesostructured TiO_2 at 380°C, mainly amorphous phase is obtained and after calcination at 500°C, the peaks at 2θ = 25.35 (101), 38.30 (103)(004)(112), 48.10 (200), 54.01 (105), 55.09 (211) and 63.23° (204) clearly reveal the presence of anatase. In the presence of Si^{4+}, whatever its content, after heating the mesostructured material at 380°C only amorphous phase is also obtained. For the TiO_2 prepared in the presence of 1 mol.% of Si^{4+} and after calcination at 500°C, the characteristic reflections of anatase are detected (Fig. 2). These peaks are quite broad, reflecting the formation of nanosized anatase. Increasing the heating temperature, the diffraction peaks become narrower, more intense and better resolved, indicating the enhancement of the crystallization degree and/or the growth of the particles. After heating at 800°C, diffraction peaks attributed to the rutile polymorph are detected at 2θ = 27.5 (110), 36 (101), 41 (111), 54.5 (211) and 57° (220). It should be noted that no trace of rutile is detected for mesostructured titania containing 10 or 20 mol.% of Si^{4+}, and besides anatase, we can also detect the presence of TiO_2-β. Indeed, for example for TiO_2 prepared in the presence of 5 mol.% of Si^{4+} and after heating at 600°C, the peaks located at 2θ = 14.5, 29.5, 33.4, 44.1 and 58° can be attributed to the (001), (-401)/ (111), (310)/(-311), (003) and (-404)/(-711) reflections of TiO_2-β [40,41]. However, higher the Si^{4+} content is, higher the temperature at which TiO_2-β appears is. For example, this phase appears after heating at 600°C and 700°C for TiO_2 containing 5 and 20 mol.% of Si^{4+}, respectively. Moreover, the higher the heteroelement content is, the more stable TiO_2-β is. TiO_2-β disappears after calcination at 800°C, when 5 mol.% of Si^{4+} have been added but it is still visible after heating after 900°C if the loading of Si^{4+} is increased to 20 mol.%. From the XRD analysis we can conclude that a delay is noted in both the amorphous to anatase (Table 1) and anatase to rutile (Table 1) transformations when the quantity of Si^{4+} is raised. Indeed, nanosized anatase is detected after calcination at 500°C and it is transformed into rutile at 800°C when 1 mol.% of Si^{4+} is introduced during the synthesis of the mesostructured TiO_2. However, when the loading of Si^{4+} reaches 20 mol.% the material remains amorphous until 700°C and the rutile polymorph is not detected, even after a treatment at 900°C. The variations of the Raman spectra as a function of both the heating temperature and the Si^{4+} loading support the conclusions arising from XRD. As a matter of fact, the bands at 141, 194, 393, 514 and 639 cm^{-1}, for the bare TiO_2 (Fig. 3), are attributed to the Eg, B_{1g}, A_{1g} or B_{1g}, and E_g modes of anatase, respectively [42]. After heating at 800°C, besides the vibration of anatase the combination band, the E_g and A_{1g} of rutile [43] appear at around 229, 445 and 605 cm^{-1} (Fig. 3), respectively. For the TiO_2 material containing 1 mol.% of Si^{4+}, a similar behavior is noted. If the Si^{4+} loading is further increased, whatever the heating temperature, the vibrations due to rutile are not observed. By contrast, the ones of TiO_2-β appear. As example, for the material containing 5 mol.% of Si^{4+}, the vibrations at 479, 364 and 237 cm^{-1} appearing after heating at 700°C are attributed to this polymorph of titania [41]. However, since Raman is seven times higher sensitive for anatase than TiO_2-β [44], it is difficult to detect the vibrations of TiO_2-β when these two forms of titania coexist.

To explain the stabilization of the mesostructure and the delay in crystallization with the increase of the Si^{4+} content, we can consider the « glass effect ». This concept has been introduced by Li et al. [45]. It consists in introducing an amorphous component designated as «glass», which acts as a glue for titania nanocrystals. The «glass» is incorporated either directly as an amorphous component [45] or by co-assembly with the amphiphiles molecules and the titania precursor [46]. In this study, samples have been prepared by co-condensation of $Ti(OiPr)_4$ and TMOS in the presence of the surfactant molecules. During the material preparation after evaporation of the solvent, titanium and silica are uniformly distributed within the P123 cylinders of the hexagonal phase and after treatment under ammonia atmosphere and surfactant extraction by ethanol.

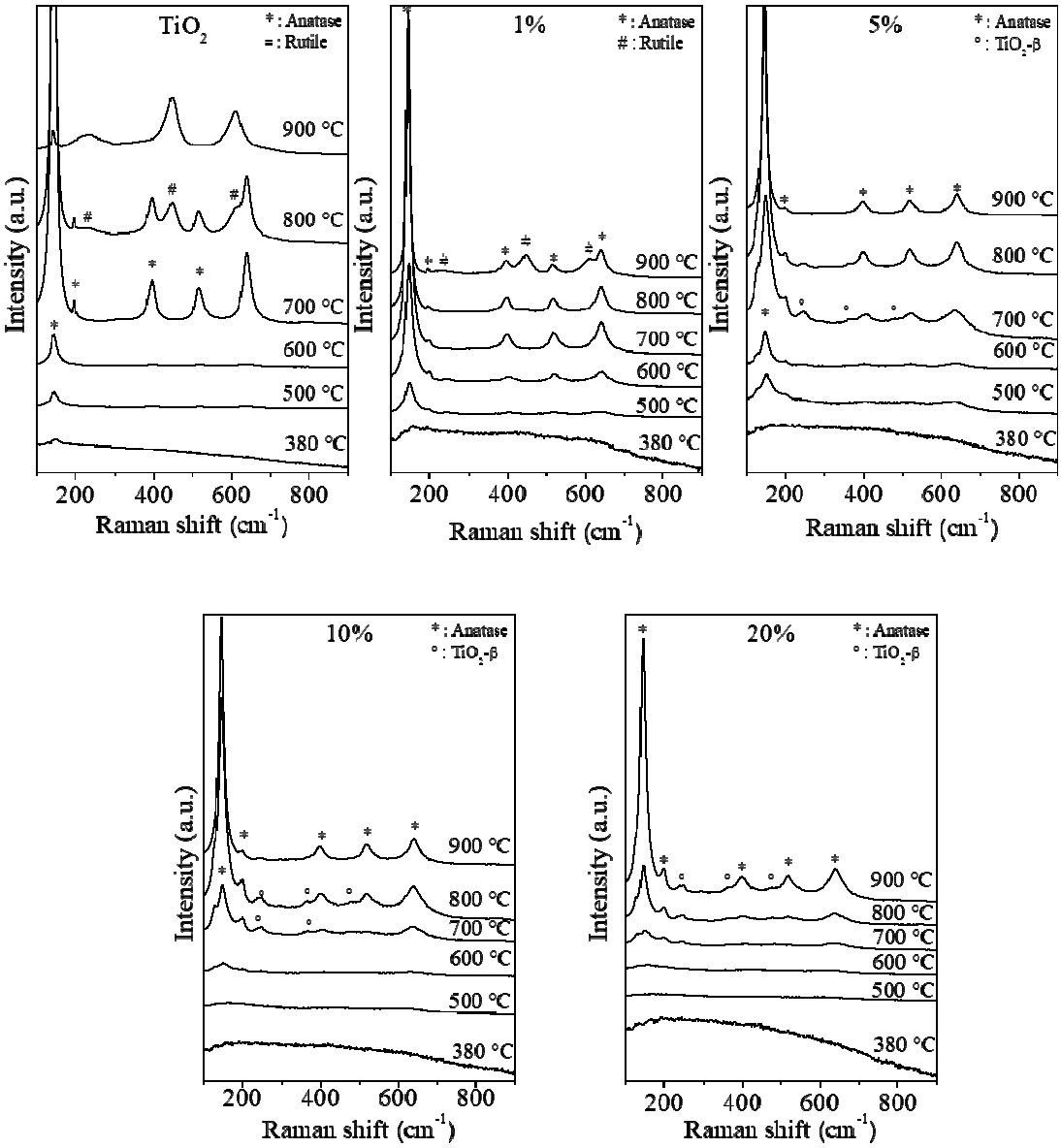

Figure 3: Evolution of the Raman spectra as a function of the heating temperature of bare TiO_2 and TiO_2 1, 5, 10 or 20 mol.% of Si^{4+}.

Amorphous matrix composed of titania and silica is obtained. During the heating process, titanium aggregates, which are surrounded by silica, are formed. Increasing the heating temperature, while titania particles begin to crystallize, silica remains amorphous. The latter acts as a binder between the anatase particles and their growth is therefore slowed down. By this way, the mesostructure is reinforced and its collapse occurs at higher temperature. The higher the Si^{4+} content, the more the « glass effect » predominates. The observation of the TiO_2-β can be also related to the « glass effect » which prevents from the transformation of TiO_2-β into anatase. Indeed, TiO_2-β is a low temperature-phase compared to anatase, and the TiO_2-β-anatase transition occurs at temperature higher than 550°C under normal pressure [47]. Stabilization of TiO_2-β up to 900°C by amorphous SiO_2 is also reported by Kogure et al. [47]. The authors succeeded in forming this phase by annealing a sol-gel derived SiO_2-TiO_2 amorphous film on a silicon wafer at 900°C in air.

3.2. Textural properties:

As long as the heating temperature remains below the one at which the mesostructured collapses, a type IV isotherm with H1 hysteresis loop is obtained by manometry nitrogen adsorption/desorption (Fig.4). After the mesostructure collapse, involved by the crystallization of the walls, the hysteresis loop progressively turned to H3. It should be noted that the temperature at which this change occurs is delayed with the increase of the heteroelement quantity (Fig. 4).

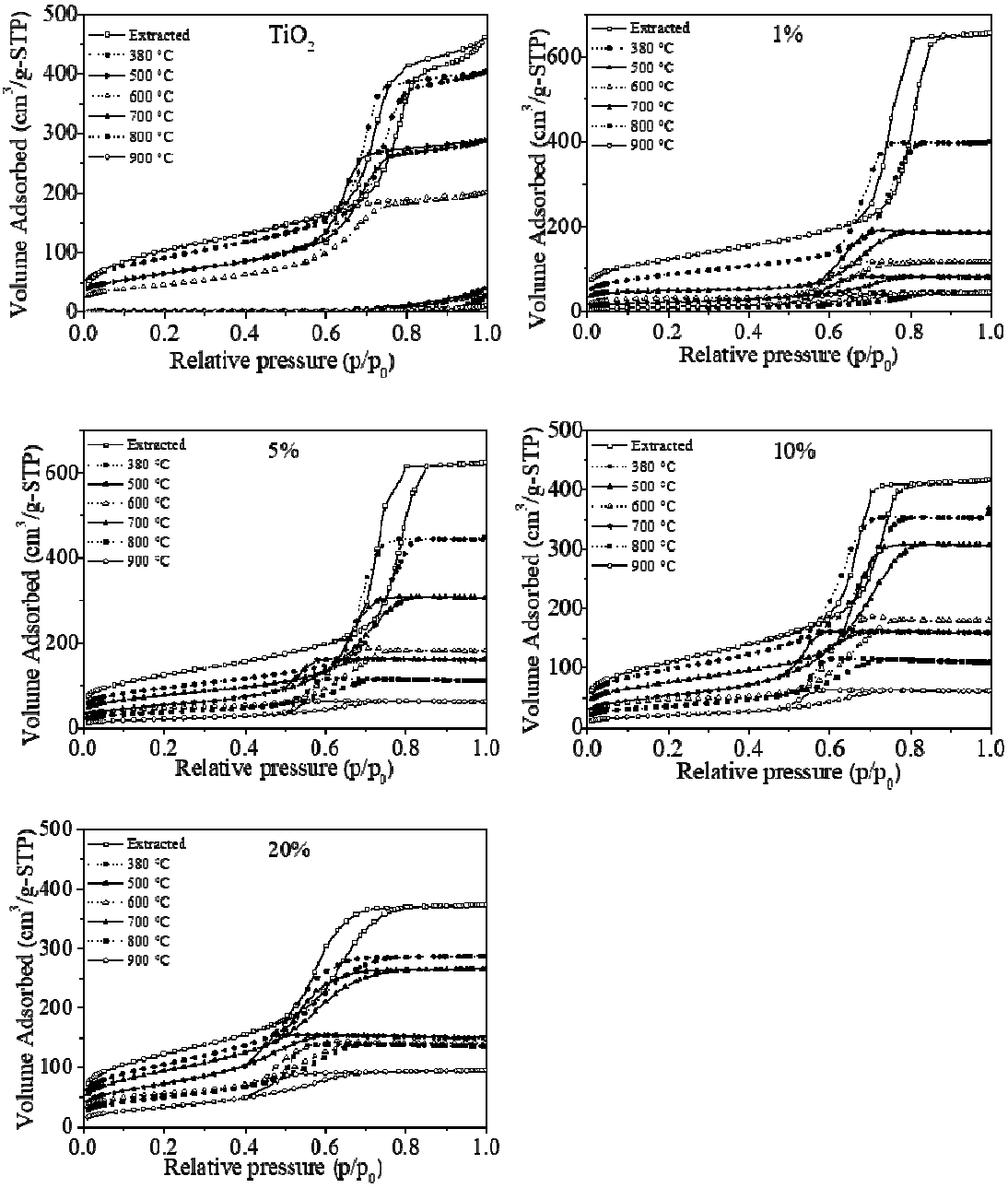

Figure 4: Nitrogen adsorption-desorption isotherms as a function of the heating temperature of bare TiO_2 and TiO_2 1, 5, 10 or 20 mol.% of Si^{4+}.

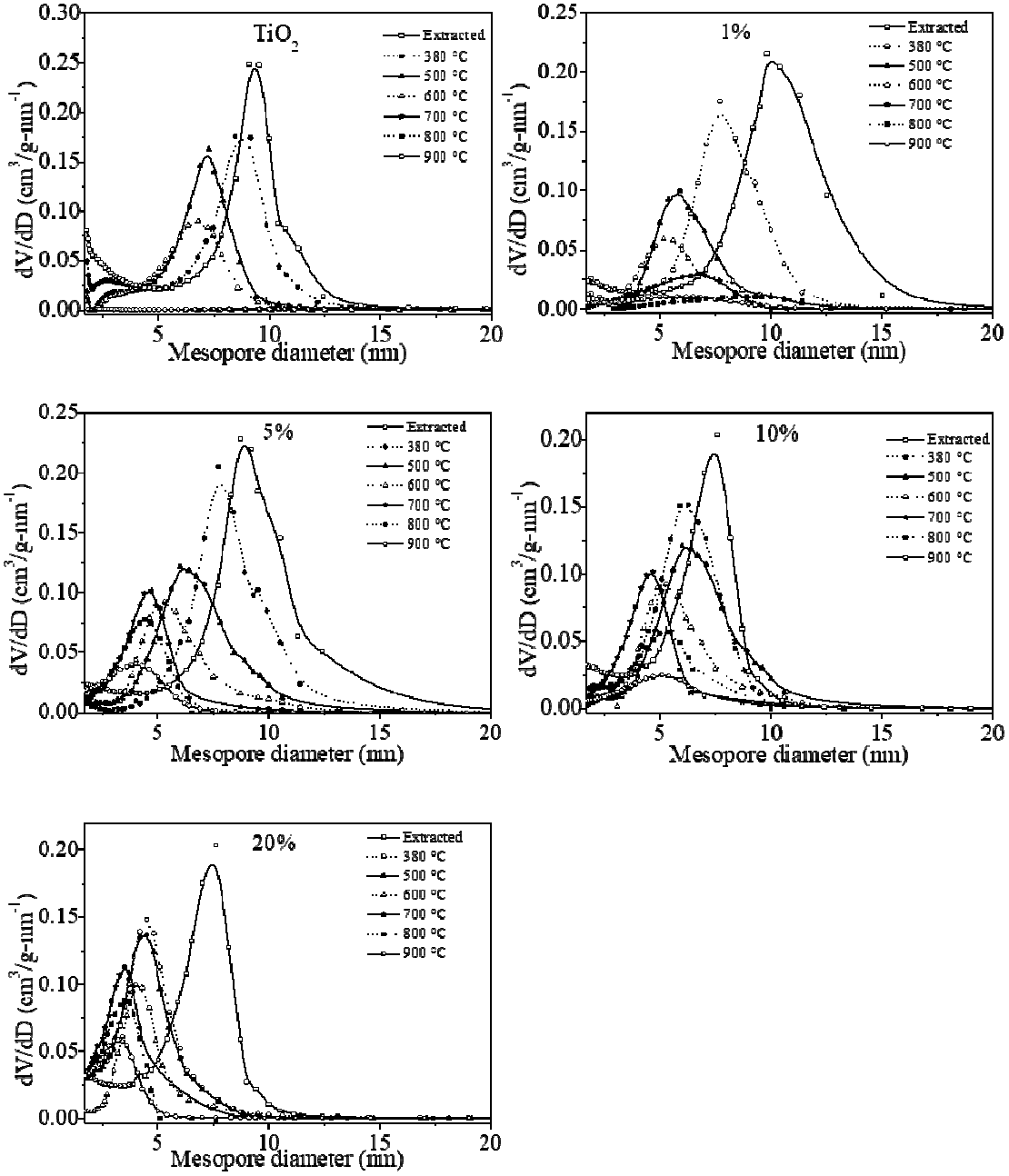

Figure 5: Mesopores size distributions as a function of the heating temperature of bare TiO_2 and TiO_2 1, 5, 10 or 20 mol.% of Si^{4+}.

Table 2: Variation of the mesopore diameter (nm) in function of the Si^{4+} loading and of the heating temperature.

Si^{4+} loading (mol.%)	Extracted	380 (°C)	500 (°C)	600 (°C)	700 (°C)	800 (°C)	900 (°C)
0	9.4	8.9	7.2	6.7	-	-	-
1	10.1	7.7	5.8	5.3	6.7	-	-
5	8.9	7.8	6.2	5.1	4.5	4.3	3.9
10	7.4	6.3	6.4	5.1	4.5	5.2	5.0
20	7.4	4.4	4.4	4.1	3.5	3.5	3.3

For the extracted samples or before the mesostructure collapse, the maximum of the mesopore size distribution is shifted towards lower mesopore diameters with the increase of the heteroelement content (Fig. 5, Table 2). The mesopore diameter of the extracted mesostructured titania containing Si^{4+} progressively decreases from 10.1 to 7.4 nm when Si^{4+} amount is varied from 1 to 20 mol.% (Table 2). This can be first due to the deformation of the lattice caused by the substitution of Ti^{4+} by the heteroelement [48]. The partial substitution of Ti^{4+} by Si^{4+} is supported by the UV-Vis spectra. As example, after heating at 380°C (Fig. 6), the UV-Vis spectrum of the bare TiO_2 exhibits a broad band that can be decomposed in two parts. The first contribution at around 245 nm arises from a ligand to metal charge transfer transition in isolated TiO_4 units. It corresponds to the band transition from Ti 3d to O 2p levels. The second contribution at 320 nm corresponds to small TiO_2 clusters [49]. The shifts noted in the presence of Si^{4+} reflects the partial substitution of Ti^{4+}. Since no pore blocking is noted on the desorption branch of the isotherms reported in Figure 4, we can also assume that the SiO_2 formed by the extra framework heteroelement envelops the mesostructured TiO_2 crystallites. The higher the Si^{4+} content is, the higher the proportion of SiO_2 is. Thus, we can assume that the surfactant cylinders are squeezed by the progressive addition of the heteroelement. This phenomenon involves a decrease of the mesopore diameter of the partially substituted mesostructured TiO_2. Finally, this variation of mesopore diameter with the increase of the Si^{4+} molar percentage also indicates the progressive transition to a different porous material induced by a higher influence of the heteroelement chemistry on the synthesis reactions. Indeed, reactivity of tetramethylorthosilicate (TMOS) is quite different than the one of titanium isopropoxide [50].

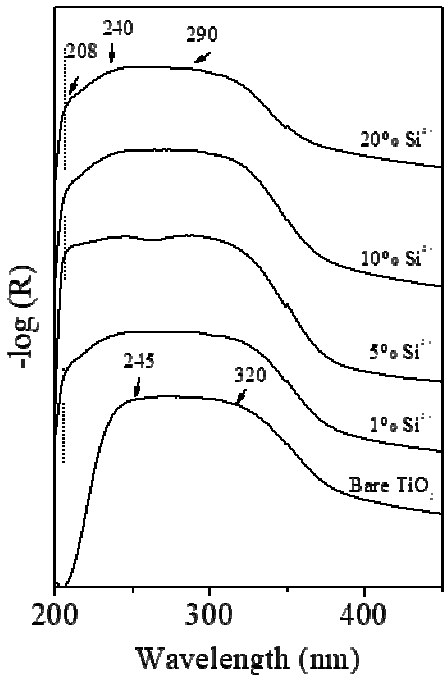

Figure 6: Diffuse reflectance UV-Visible spectrum of the bare mesostructured titania and containing 1, 5, 10 or 20 mol.% of Si^{4+}. Samples have been heated at 380°C.

When the mesostructure has begun to collapse, the dV/dD values decrease, the pore size distribution becomes very broad (Fig. 5). For all samples, because of the walls crystallization the specific surface area and the pore volume gradually decrease with temperature (Fig. 7). After heating at high temperature, the specific surface area of the materials prepared in the

presence of 10 or 20 mol.% of Si^{4+} remains relatively high, respectively 130 and 170 m²/g after heating at 900°C (Fig. 7.). This further shows the protector effect of SiO_2.

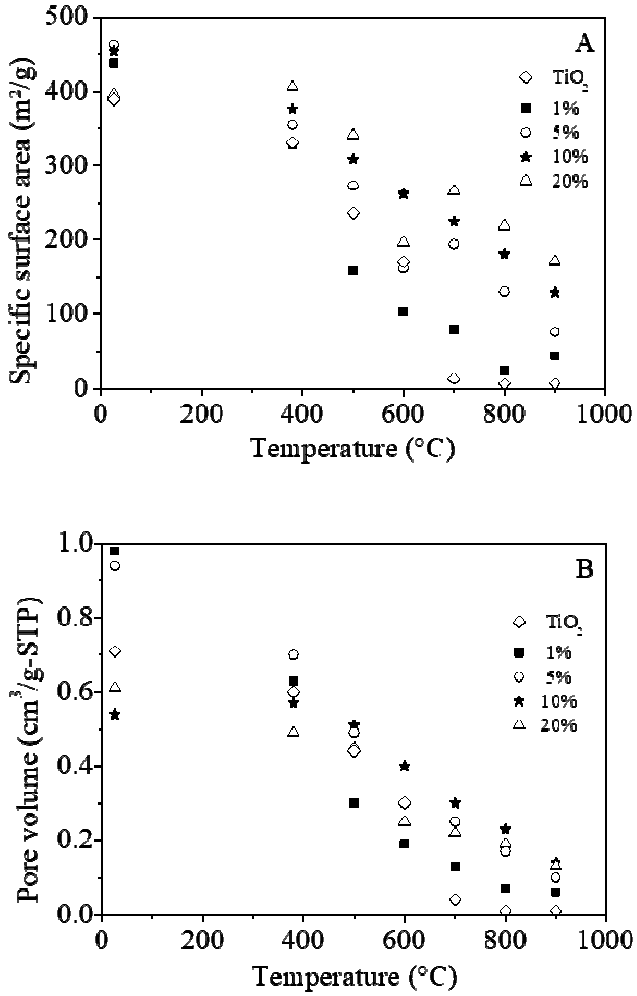

Figure 7: Variation of the specific surface area (A) and of the pore volume (B) as a function of the heating temperature of TiO_2 containing 1, 5, 10 or 20 mol.% of Si^{4+}.

3.3. Photodegradation of methyl orange:

From the UV spectra, the band gap values have been calculated using the Kubelka-Munk function from a plot of $(\alpha h\nu)^2$ versus photon energy ($h\nu$), where α stands the adsorption coefficient. The band gap (E) is determined by extrapolating the straight-line portion of $(\alpha h\nu)^{1/2} = 0$ axis. The intercept of the tangent of the plot gives the value of E. Results are depicted in Figure 8. In a general way, increasing the heating temperature leads to a decrease of E. For example, for TiO_2 containing 1 mol.% of Si^{4+}, E varies from 3.21 to 2.95 eV if the heating temperature is changed from 380 to 900°C. This behavior can be correlated to various factors. First, as observed by SAXS and XRD, with the increase of the heating temperature, the anatase particles grow. Their size (diameter = 2R) has been determined with the Scherrer equation (Table 3) and compared to the Bohr radius of the exciton (a_{Bohr}), which has been taken equal to 3.2 nm according to the study reported by Baldini et al. [51]. As the radius of the particle approaches the Bohr radius of the exciton, quantization of the energy bands becomes apparent and a blue shift in the exciton transition energy can be observed [52].

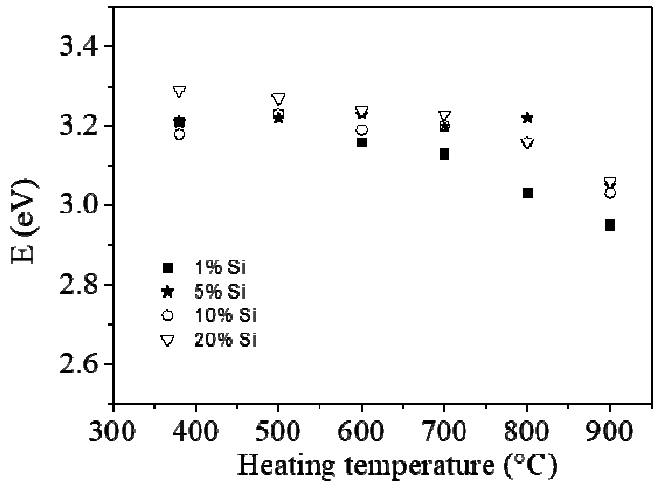

Figure 8: Variation of the energy band gap (E) as a function of the heating temperature of TiO_2 containing 1, 5, 10 or 20 mol.% of Si^{4+}.

Table 3: Crystallites sizes of anatase 2R (nm) determined with Scherrer equation in function of the Si^{4+} loading and of the heating temperature.

Si^{4+} loading (mol.%)	380 (°C)	500 (°C)	600 (°C)	700 (°C)	800 (°C)	900 (°C)
0	2	8	10	71^{R}	543^{R}	291^{R}
1	-	5^{β}	8^{β}	15	35^{R}	34^{R}
5	-	3	5^{β}	6^{β}	11^{β}	20^{R}
10	-	-	2	4^{β}	8^{β}	13
20	-	-	-	3^{β}	5^{β}	7^{β}

- : no observable anatase crystallites
^{R} : rutile
$^{\beta}$: β-TiO_2

It is reported that if $R > a_{Bohr}$, a weak confinement regime is noted, whereas a strong one is observed if $R < a_{Bohr}$ [53]. Increasing the heating temperature from 380 to 900°C, the size of the crystallites (2R) increases from 5 to 34 nm (Table 3). The R values become higher than a_{Bohr} and in that case the size quantification effect is reduced as a consequence the band gap decreases. Second, the variation of E also reflects the contribution of TiO_2-β, which has a bandgap energy lower than the anatase phase [54]. Third, for the titania prepared in the presence of 1 mol.% of Si^{4+}, rutile is detected after heating at 800°C. The narrow bandgap energy of rutile around 3.0 eV [55] contributes to further decrease E for this sample. Due to the fact that, with the increase of Si^{4+} content, both the appearance of rutile and the growth of the anatase particles are delayed due to the « glass effect » (Table 3), for a given heating temperature, overall, materials prepared with a higher Si^{4+} content have a higher energy bandgap value. For example, after heating at 700°C, the size of the anatase crystallite decreases from 15 to 3 nm by increasing the Si^{4+} content from 1 to 20 mol.% and E increases from 3.13 to 3.23 eV.

The dependence of the heating temperature on the time course of the photocatalytic degradation of methyl orange, used as a model dye, is illustrated in Figure 9 for titania synthesized in the presence of 1 (Fig. 9A) and 10 (Fig.9B) mol.% of Si^{4+}, respectively. Each curve shows the bulk concentration of methyl orange as a function of the irradiation time.

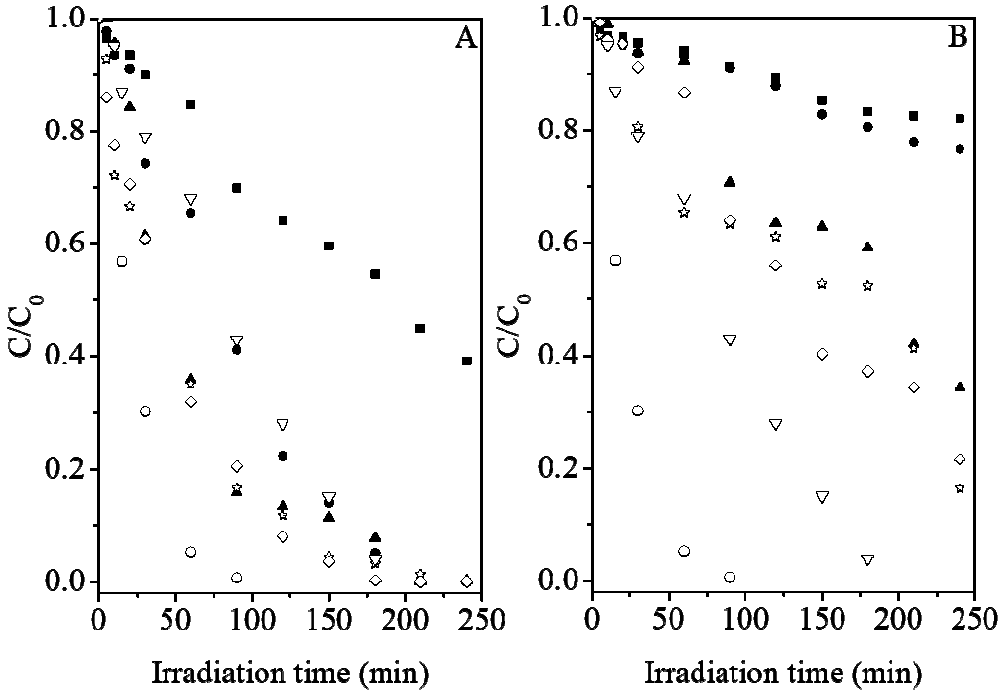

Figure 9: Relative methyl orange concentration versus irradiation time. The photocatalysts have been prepared in the presence of 1 (A) or 10 mol.% (B) of Si^{4+}. Materials have been heated at 380 (■), 500 (●), 700 (▲), 800 (◇) or 900 °C (★). P25 (○) and anatase 10 nm (▽) are used as pure TiO_2 reference materials.

For materials containing 1 mol.% of Si^{4+} (Fig. 9A), the lowest photocatalytic activity is noted after heating at 380°C. This can be relied to the fact that for this sample, only amorphous phase has been detected by XRD and Raman. Indeed, the amorphous phase comprises numerous defects, i.e., impurities, dangling bonds, and microvoids that can behave as recombination centers for the photoinduced electron/hole (e−/h+) pairs [56]. If the heating temperature is increased, the efficiency in decolorizing the dye solution also increases until it reaches its maximum after heating at 800°C. In that case, after 90 minutes, 80% of the dye solution is discolored, and it is completely discolored after 180 min. This enhancement of the photocatalytic efficiency can be correlated with the appearance of the anatase particles and their growth as observed by XRD. Indeed, the photocatalytic activity of TiO_2 is mainly attributed to its anatase phase and it is reported that higher crystallinity enhances drastically the photocatalytic activity of TiO_2 materials [56,57]. The presence of nanocrystalline anatase decreases the number of lattice defects and then facilitates the electron transport for reacting with water and methyl orange molecules adsorbed on the TiO_2 surface along the mesopore structure, leading to much better photocatalytic performance [58]. After heating at 800°C, the rutile phase begins to appear and it induces a decrease of the bandgap energy to 2.95 eV after heating at 900°C (Fig. 8). The lower value of E is an unfavorable parameter for photocatalysis under UV radiation. This favors the recombination of electron/hole pairs and the photocatalytic efficiency of the material decreases.

Looking at the activity of the mesostructured titania containing 10 mol.% of Si^{4+} (Fig. 9B), samples heated at 380 and 500°C show the lowest photocatalytic activity with a maximum of 20% discoloration of the solution after 240 minutes. As the heating temperature increases, the efficiency for the discoloration of the solution also increases. With about 80% of discoloration

after 240 minutes, the maximum is obtained for the material heated at 900°C. Once again, the increase in efficiency is in accordance with the crystallization of anatase. Indeed, as explained above, thanks to the « glass effect », increasing the Si^{4+} content delays the crystallization of the mesopore framework and the complete transformation of TiO_2-β into anatase.
The curves C/C_0 as a function of irradiation time for commercial TiO_2 sample (P25 : 70% anatase, 30% rutile from Evonik and pure anatase from Alfa Aesar) are also reported in Figure 9 for comparison. Whatever the heating temperature and the Si^{4+} content, the photoactivity of mesostructured titania containing Si^{4+} is lower than P25. This difference can be partly explained by the different amounts of anatase in the mesostructured TiO_2 solids but also by the synergic positive effect of the anatase/rutile mixture on the photocatalytic activity of TiO_2. Indeed, it has been shown that a mixture of anatase and rutile crystallites had better photocatalytic activity than that of pure anatase or pure rutile [59]. Compared to commercial anatase from Alfa Aesar, the photoactivity of mesostructured TiO_2 containing 1 mol.% of Si^{4+} and heating at temperature higher than 380°C is in the same range of order or higher than the one of the commercial titania. This can be attributed to the growth of the anatase particles as observed by XRD and Raman analysis. Indeed, crystallite size was also reported as a predominant factor for photocatalytic activity with improvement of the photocatalysis efficiency when crystallite size decreases. If the mesostructured TiO_2 contains 10 mol.%, since the crystallization of the walls and the growth of the particles are delayed, whatever the heating temperature, the photocatalytic activity is lower than the one of commercial anatase from Alfa Aesar.
Results reported here for methyl orange are in good accordance with the ones obtained by Kusakabe et al [60] for the photodegradation of methyl blue using silica-loaded mesoporous titania composite. The authors report that highest activity is obtained for low silica content composite. However, the authors have not made correlation between the photocatalytic activity and the crystallographic phase formed or with the bandgap energy, which has not been evaluated.
The degradation experiments by UV irradiation of methyl orange solutions containing the TiO_2-based photocatalysts are expected to follow the pseudo-first-order kinetics with respect to the methyl orange concentration in the bulk solution (C):

$$-\frac{dC}{dt} = k_{app} C \qquad (1)$$

Integration of that equation, considering that $C = C_0$ at $t = 0$, with C_0 being the initial concentration in the bulk solution after dark adsorption and t the reaction time, leads to:

$$\ln\left(\frac{C_0}{C}\right) = k_{app} t \qquad (2)$$

where k_{app} stands for the apparent pseudo-first-order rate constant.
The values of k_{app} can be obtained directly from the regression analysis of the linear curve in the plot. All the results are shown in Figure 10. For materials containing 1 mol.% of Si^{4+}, the photocatalytic rate constant first increases up to a heating temperature of 500 °C and then when the anatase phase is present, it remains almost constant around a value of 0.022 min^{-1}. Its value slightly decreases after heating at 900°C, when rutile has appeared. By contrast, when titania containing 10 mol.% of Si^{4+} is used as photocatalyst, k_{app} continuously increases but its value is much low than the one obtained using mesostructured TiO_2 containing 1 mol.% of Si^{4+}. For the photocatalysts obtained after heating at 900°C, there is a factor of 10 between the two values of k_{app} which are 0.020 and 0.002 min^{-1}, respectively. In these materials, the delay in the crystallization evidenced by XRD and Raman is therefore detrimental to the discoloration of the dye solution since the appearance of the most photoactive phase, anatase is delayed as the growth of the particles.

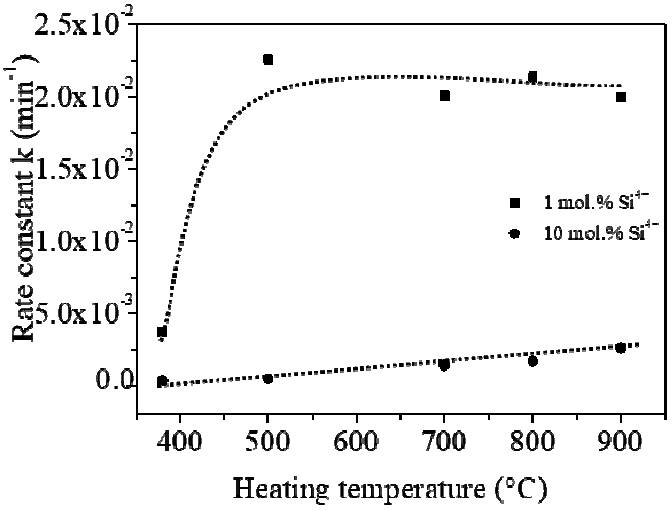

Figure 10: Variation of the degradation rate as a function of the heating temperature. The photocatalysts have been prepared in the presence of 1 or 10 mol.% of Si^{4+}. Lines are just a guide for the eyes.

4. Conclusions

When preparing mesostructured TiO_2, because of the intrinsical crystallization of anatase, the mesostructure collapses and most of the porosity is lost after being heated at 300-350 °C. Here, to reinforce the mesostructured framework, TiO_2-SiO_2 composites have been prepared by the co-condensation of titanium isopropoxide and tetramethylorthosilicate in the presence of the triblock copolymer Pluronic P123.

Results obtained by SAXS, X-Ray diffraction, Raman spectroscopy and manometry nitrogen adsorption-desorption show that, thanks to the protector role played by the amorphous SiO_2 surrounded the titania crystallites and by comparison with the bare mesostructured titania, the crystallization is delayed and the growth of the anatase particles is limited. The transformation from anatase to rutile also occurs at higher temperature and the TiO_2-β phase is stabilized. However, as a consequence of the beneficial effect of presence of the heteroelement on the thermal stability of titania, the efficiency of the prepared materials for the discoloration of methyl orange solution under UV light is inhibited since the latter delays both the appearance of anatase and the growth of the particles. Indeed, the photocatalytic efficiency of TiO_2 in solution is strongly associated to its anatase phase and higher crystallinity enhanced drastically the photocatalytic activity.

Credit authorship contribution statement

Bénédicte Lebeau: Writing - original draft, Supervision. Florian Jonas: Investigation. Laure Michelin: Investigation. Jean-Luc Blin: Writing - original draft, Supervision.

Conflicts of interest

The authors declare that they have no competing interests

Acknowledgments

We would like to thank the platform "Spectroscopies et Microscopies des Interfaces" from LCPME. The platform "X-Ray Diffraction" of IS2M is also acknowledged. Florian Jonas thanks the « Region Grand-Est » for the financial support of his PhD.

Funding:
This work was supported by the « Region Grand-Est » [grant number RPHPHXAS-D-AOT17-TITAN].

References

[1] U.P.M. Ashik, A. Viswan, S. Kudo, J.I. Hayashi, Nanomaterials as Catalysts, in: S.M. Bhagyaraj O.S. Oluwafemi, N. Kalarikkal, S. Thomas (Eds.), Applications of Nanomaterials, Woodhead Publishing, Duxford, 2018, pp. 45-82.

[2] D. Trong On, D. Desplantier-Giscard, C. Danumah, S. Kaliaguine, Perspectives in catalytic applications of mesostructured materials, Appl. Catal., A 253 (2003) 545-602.

[3] C. Perego, R. Millini, Porous materials in catalysis: challenges for mesoporous materials, Chem. Soc. Rev. 42 (2013) 3956-3976.

[4] Z. Ma, B. Zhou, Y. Ren, Crystalline mesoporous transition metal oxides: hard-templating synthesis and application in environmental catalysis ; Front. Environ. Sci. Eng. 7 (2013) 341-355.

[5] F. Schüth, Non-siliceous mesostructured and mesoporous materials, Chem. Mater. 13 (2001) 13, 3184-3195.

[6] C. Yu, B. Tian, D. Zhao, Recent advances in the synthesis of non-siliceous mesoporous materials, Curr. Opin. Solid State Mater. Sci. 7 (2003) 191-197.

[7] D Gu, F. Schüth, Synthesis of non-siliceous mesoporous oxides, Chem. Soc. Rev., 43 (2014) 43 313-344.

[8] T. Kimura, Evaporation-induced Self-assembly Process Controlled for Obtaining Highly Ordered Mesoporous Materials with Demanded Morphologies Chem. Rec., 16 (2016) 445-457.

[9] C. Sanchez, F. Ribot, Design of hybrid organic-inorganic materials synthesized via sol-gel chemistry, New J. Chem. 18 (1994) 1007-1047.

[10] Y. Bai, I. Mora-Seró, F. De Angelis, J. Bisquert, P. Wang, Titanium dioxide nanomaterials for photovoltaic applications, Chem. Rev. 114 (2014) 10095-10130.

[11] Y. Ma, W. Wang, Y. Jia, X. Chen, H. Han, C. Li, Titanium dioxide-based nanomaterials for photocatalytic fuel generations, Chem. Rev. 114 (2014) 9987-10043.

[12] K.I. Hadjiivanov, D.G. Klissurski, Surface chemistry of titania (anatase) and titania-supported catalysts, Chem. Soc. Rev. 25 (1996) 61-69.

[13] O. Carp, C.L. Huisman, A. Reller, Photoinduced reactivity of titanium dioxide, Prog. Solid State Chem. 32 (2004) 33-177.

[14] M. Fox, M. Dulay, Heterogeneous Photocatalysis, Chem. Rev., 1993, 93, 341-357.

[15] M. Pelaez, N.T. Nolan, S.C. Pillai, M.K. Seery, P. Falaras, A.G. Kontos, P.S.M. Dunlop, J.W.J. Hamilton, J.A. Byrne, K. O'Shea, M.H. Entezari, D.D. Dionysiou, A review on the visible light active titanium dioxide photocatalysts for environmental applications, Appl. Catal. B Environ. 125 (2012) 331-349.

[16] M. Hoffmann, M. S. Martin, W. Choi , D. Bahnemann, Environmental Applications of Semiconductor Photocatalysis, Chem. Rev. 95 (1995) 69-96.

[17] U.I. Gaya, A.H. Abdullah, Heterogeneous photocatalytic degradation of organic contaminants over titanium dioxide: A review of fundamentals, progress and problems, J. Photochem. Photobiol. C 9 (2008) 1-12.

[18] Z. Li, B. Hou, D. Xu, D. Wu, Y. Sun, Hydrothermal synthesis, characterization, and photocatalytic performance of silica-Modified titanium dioxide nanoparticles, J. Colloid Interface Sci. 288 (2005) 149-154.

[19] D.S. Kim, S.J. Han, S.Y. Kwak, Synthesis and photocatalytic activity of mesoporous TiO_2 with the surface area, crystallite size, and pore size, J. Colloid. Interface Sci. 316 (2007) 85-91.

[20] W.F. Zhang, Y.L. He, M.S. Zhang, Z. Yin, Q. Chen, Raman scattering study on anatase TiO_2 nanocrystals, J. Phys. D: Appl. Phys. 33 (2000) 912-916.

[21] W. Li, Z. Wu, J. Wang, A.A. Elzatahry, D. Zhao, A perspective on mesoporous TiO_2 materials, Chem. Mater. 26 (2014) 287-298.
[22] S. Bagheri, Z.A.M. Hir, A.T. Yousefi, S.B.A. Hamid, Progress on mesoporous titanium dioxide: synthesis, modification and applications, Microporous Mesoporous Mater. 218 (2015) 206-222.
[23] Md. K. Hossain, U.S. Akhtar, A.R. Koirala, I.C. Hwang, K.B. Yoon, Steam-assisted synthesis of uniformly mesoporous anatase and its remarkably superior photocatalytic activities, Catal. Today, 243 (2015) 228-234.
[24] S.C. Zi, S. Chandren, L.S. Yuan, R. Razali, C.S. Ho, D. Hartanto, T.M.I. Mahlia, H. Nur, New method to synthesize mesoporous titania by photodegradation of surfactant template, Solid State Sci. 52 (2016) 83-91.
[25] J. Li, Y. Chen, Y. Wang, Z. Yan, D. Duan, J. Wang, Synthesis; photocatalysis of mesoporous titania templated by natural rubber latex. RSC Adv. 5 (2015) 21480-21486.
[26] S. Rasalingam, C.M. Wu, R.T. Koodali, Modulation of pore sizes of titanium dioxide photocatalysts by a facile template free hydrothermal synthesis method: Implications for photocatalytic degradation of Rhodamine B, ACS Appl. Mater. Interfaces 7 (2015) 4368-4380.
[27] K. Zimny, J. Ghanbaja, C. Carteret, M.J. Stébé, J.L. Blin, Highly ordered mesoporous titania with semi crystalline framework templated by large or small nonionic surfactants, New. J. Chem. 34 (2010) 2113-2117.
[28] K. Zimny, T. Roques-Carmes, C. Carteret, M.J. Stébé, J.L. Blin, Synthesis and photoactivity of ordered mesoporous titania with a semicrystalline framework, J. Phys. Chem. C 116 (2012) 6585-6594.
[29] J.L. Blin, M.J. Stébé, T. Roques-Carmes, Use of ordered mesoporous titania with semi-crystalline framework as photocatalyst, Colloids Surf., A 407 (2012) 177-185.
[30] I. Naboulsi, B. Lebeau, L. Michelin, C. Carteret, L. Vidal, M. Bonne, J.L. Blin, Insights into the formation and properties of templated dual mesoporous titania with enhanced photocatalytic activity, ACS Appl. Mater. Interfaces 9 (2017) 3113-3122.
[31] S.Y. Choi, M. Mamak, N. Coombs, N. Chopra, G.A. Ozin, Thermally stable two-dimensional hexagonal mesoporous nanocrystalline anatase, Meso-nc-TiO_2: bulk and crack-free thin film morphologies, Adv. Funct. Mater. 14 (2004) 355-344.
[32] D.L. Li, H.S. Zhou, I. Homma, Design and synthesis of self-ordered mesoporous nanocomposite through controlled in-situ crystallization, Nat. Mater. 3 (2004) 65-72.
[33] Y. Zhang, H. Zhang, Y. Xu, Y. Wang, Significant effect of lanthanide doping on the texture and properties of nanocrystalline mesoporous TiO_2, J. Solid State Chem. 177 (2004) 3490-3498.
[34] W. Dong, Y. Sun, C.W. Lee, W. Hua, X. Lu, Y. Shi, S. Zhang, J. Chen, D. Zhao, Controllable and repeatable synthesis of thermally stable anatase nanocrystal-silica composites with highly ordered hexagonal mesostructures, J. Am. Chem. Soc. 129 (2007) 13894-13904.
[35] W. Dong, Y. Sun, Q. Ma., L. Zhu, W. Hua, X. Lu, G. Zhuang, S. Zhang, Z. Guo, D. Zhao, Excellent photocatalytic degradation activities of ordered mesoporous anatase TiO_2-SiO_2 nanocomposites to various organic contaminants, J. Hazardous Mater. 229-230 (2012) 307-320.
[36] D.L. Liao, C.A. Badour, B.Q. Liao, Preparation of Nanosized TiO_2/ZnO Composite Catalyst and its Photocatalytic Activity for Degradation of Methyl Orange, J. Photochem. Photobiol. A Chem. 194 (2008) 11-19.

[37] P. Periyat, K.V. Baiju, P. Mukundan, P.K. Pillai, K.G.K. Warrier, High temperature stable mesoporous anatase TiO_2 photocatalyst achieve by silicon addition, Appl. Catal., A 349 (2008) 13-19.
[38] K. Assaker, B. Lebeau, L. Michelin, P. Gaudin, C. Carteret, L. Vidal, M. Bonne, J.L. Blin, Zn-TiO_2 mesoporous oxides prepared by mechanical milling, J. Alloys Compd. 649 (2015) 1-10.
[39] M. Thommes, K. Kaneko, A. V. Neimark, J. P. Olivier, F. Rodriguez-Reinoso, J. Rouquerol, K. S. W. Sing, Physisorption of gases, with special reference to the evaluation of surface area and pore size distribution (IUPAC Technical Report), Pure Appl. Chem. 87 (2015) 1051-1069.
[40] M.Y. Manuputty, J.A.H. Dreyer, Y. Sheng, E.J. Bringley, M.L. Botero, J. Akroyd, M. Kraft, Polymorphism of nanocrystalline TiO_2 prepared in a stagnation flame: formation of the TiO_2-II phase, Chem. Sci. 10 (2019) 1342-1350.
[41] G. Wang, Z.Y. Liu, J.N. Wu, Q. Lu, Preparation and electrochemical capacitance behavior of TiO_2 -B nanotubes for hybrid supercapacitor, Mater. Lett. 71 (2012) 120-122.
[42] S. Kelly, F.H. Pollak, M. Tomkiewicz, Raman spectroscopy as a morphological probe for TiO_2 aerogels, J. Phys. Chem. B 101 (1997) 2730-2734.
[43] A. Mattsson, L. Österlund, Phys. Chem. C, Adsorption and photoinduced decomposition of acetone and acetic acid on anatase, brookite, and rutile TiO_2 nanoparticles 114 (2010) 14121-14132.
[44] T. Beuvier, M. Richard-Plouet, L. Brohan, Accurate methods for quantifying the relative ratio of anatase and TiO_2(B) nanoparticles, J. Phys. Chem. C 113 (2009) 13703-13706.
[45] D. L. Li, H.S. Zhou, I. Homma, Design and synthesis of self-ordered mesoporous nanocomposite through controlled in-situ crystallization, Nat. Mater. 3 (2004) 65-72.
[46] R. Liu, Y. Ren, Y. Shi, F. Zhang, L. Zhang, B. Tu, Controlled synthesis of ordered mesoporous C–TiO_2 nanocomposites with crystalline titania frameworks from organic–inorganic–amphiphilic coassembly, Chem. Mater. 20 (2008) 1140-1146.
[47] T. Kogure, T. Umezawa, Formation of TiO_2(B) nanocrystallites in sol–gel-derived SiO_2–TiO_2 film, J. Am. Ceram. Soc. 82 (1999) 3248-50.
[48] R. Rodríguez-Talavera, S. Vargas, R. Arroyo-Murillo, R. Montiel-Campos, E. Haro-Poniatowski, Modification of the phase transition temperatures in titania doped with various cations, J. Mater. Res. 12 (1997) 439-443.
[49] L.G. Devi, N. Kottam, B.N. Murthy, S.G. Kumar, Enhanced photocatalytic activity of transition metal ions Mn^{2+}, Ni^{2+} and Zn^{2+} doped polycrystalline titania for the degradation of aniline blue under UV/solar light, J. Mol. Catal. A Chem. 328 (2010) 44-52.
[50] P. Judeinstein, C. Sanchez, Hybrid organic-inorganic materials: a land of multidisciplinarity, J. Mater. Chem. 6 (1996) 511-525.
[51] E. Baldini, L. Chiodo , A. Dominguez, M. Palummo, S. Moser, M. Yazdi-Rizi, G. Auböck, B.P.P. Mallett, H. Berger, A. Magrez, C. Bernhard, M. Grioni, A. Rubio, M. Chergui, Strongly bound excitons in anatase TiO_2 single crystals and nanoparticles, Nat. Commun. 8 (2017) 13.
[52] Y. W., N. Herron, Quantum size effects on the exciton energy of CdS clusters, Phys. Rev. B 42 (1990) 7253-7255.
[53] S. Monticone, R. Tufeu, A.V. Kanaev, E. Scolan, C. Sanchez, Quantum size effect in TiO_2 nanoparticles: does it exist?, Appl. Surf. Sci. 162-163 (2000) 565-570.

[54] T. Peng, S. Ray, S. S. Veeravalli, J. A. Lalmana, F. Arefi-Khonsari, The role of hydrothermal conditions in determining 1D TiO_2 nanomaterials bandgap energies and crystal phases, Mater. Res. Bull. 105 (2018) 104-113.
[55] D. Reyes-Coronado, G. Rodriguez-Gattorno, M.E. Espinosa-Pesqueira, C. Cab, R. de Coss, G. Oskam, Phase-pure TiO_2 nanoparticles: anatase, brookite and rutile, Nanotechnology 19 (2008) 145605.
[56] B. Ohtani, Y. Ogawa, S. Nishimoto, Photocatalytic activity of amorphous-anatase mixture of titanium(IV) oxide particles suspended in aqueous solutions, J. Phys. Chem. B 101 (1997) 3746-3752.
[57] W.F. Zhang, Y.L. He, M.S. Zhang, Z. Yin, Q. Chen, Raman scattering study on anatase TiO_2 nanocrystals, J. Phys. D: Appl. Phys 33 (2000) 912-916.
[58] T. Sreethawong, Y. Suzuki, S. Yoshikawa, Photocatalytic evolution of hydrogen over nanocrystalline mesoporous titania prepared by surfactant-assisted templating sol–gel process, Catalysis comm. 6 (2005) 119124.
[59] T. Ohno, K. Tokieda, S. Higashida, M. Matsumura, Synergism between rutile and anatase TiO_2 particles in photocatalytic oxidation of naphthalene, Appl. Catal. A: Gen. 244 (2003) 383-391.
[60] K. Kusakabe, M. Ezaki, A. Sakoguchi, K. Oda, N. Ikeda, Photocatalytic behaviors of silica-loaded mesoporous titania, Chem. Eng. J. 180 (2012) 245-249.

Figures caption

Figure 1: Evolution of the SAXS pattern as a function of the heating temperature of bare TiO_2 and TiO_2 containing 1, 5, 10 or 20 mol.% of Si^{4+}.

Figure 2: Evolution of the X-Ray diffractogramms as a function of the heating temperature of bare TiO_2 and TiO_2 1, 5, 10 or 20 mol.% of Si^{4+}.

Figure 3: Evolution of the Raman spectra as a function of the heating temperature of bare TiO_2 and TiO_2 1, 5, 10 or 20 mol.% of Si^{4+}.

Figure 4: Nitrogen adsorption-desorption isotherms as a function of the heating temperature of bare TiO_2 and TiO_2 1, 5, 10 or 20 mol.% of Si^{4+}.

Figure 5: Mesopores size distributions as a function of the heating temperature of bare TiO_2 and TiO_2 1, 5, 10 or 20 mol.% of Si^{4+}.

Figure 6: Diffuse reflectance UV-Visible spectrum of the bare mesostructured titania and containing 1, 5, 10 or 20 mol.% of Si^{4+}. Samples have been heated at 380°C.

Figure 7: Variation of the specific surface area (A) and of the pore volume (B) as a function of the heating temperature of TiO_2 containing 1, 5, 10 or 20 mol.% of Si^{4+}.

Figure 8: Variation of the energy band gap (E) as a function of the heating temperature of TiO_2 containing 1, 5, 10 or 20 mol.% of Si^{4+}.

Figure 9: Relative methyl orange concentration versus irradiation time. The photocatalysts have been prepared in the presence of 1 (A) or 10 mol.% (B) of Si^{4+}. Materials have been heated at 380 (■), 500 (●), 700 (▲), 800 (◇) or 900 °C (✯). P25 (○) and anatase 10 nm (▽) are used as pure TiO_2 reference materials.

Figure 10: Variation of the degradation rate as a function of the heating temperature. The photocatalysts have been prepared in the presence of 1 or 10 mol.% of Si^{4+}. Lines are just a guide for the eyes.

Table 1: Collapse temperature (T_C) of the mesostructure, temperature of crystallization into nanosized anatase (T_A), temperature at which the rutile polymorph is detected (T_R) as a function the Si content (mol.%).

Si^{4+} loading (mol.%)	T_C (°C)	T_A (°C)	T_R (°C)
0	600	380	700
1	500	500	800
5	700	500	-
10	700	600	-
20	900	700	-

Table 2: Variation of the mesopore diameter (nm) in function of the Si^{4+} loading and of the heating temperature.

Si^{4+} loading (mol.%)	Extracted	380 (°C)	500 (°C)	600 (°C)	700 (°C)	800 (°C)	900 (°C)
0	9.4	8.9	7.2	6.7	-	-	-
1	10.1	7.7	5.8	5.3	6.7	-	-
5	8.9	7.8	6.2	5.1	4.5	4.3	3.9
10	7.4	6.3	6.4	5.1	4.5	5.2	5.0
20	7.4	4.4	4.4	4.1	3.5	3.5	3.3

Table 3: Crystallites sizes of anatase 2R (nm) determined with Scherrer equation in function of the Si^{4+} loading and of the heating temperature.

Si^{4+} loading (mol.%)	380 (°C)	500 (°C)	600 (°C)	700 (°C)	800 (°C)	900 (°C)
0	2	8	10	71^{R}	543^{R}	291^{R}
1	-	5^{β}	8^{β}	15	35^{R}	34^{R}
5	-	3	5^{β}	6^{β}	11^{β}	20^{R}
10	-	-	2	4^{β}	8^{β}	13
20	-	-	-	3^{β}	5^{β}	7^{β}

- : no observable anatase crystallites
^{R} : rutile
$^{\beta}$: β-TiO_2

Figure 1

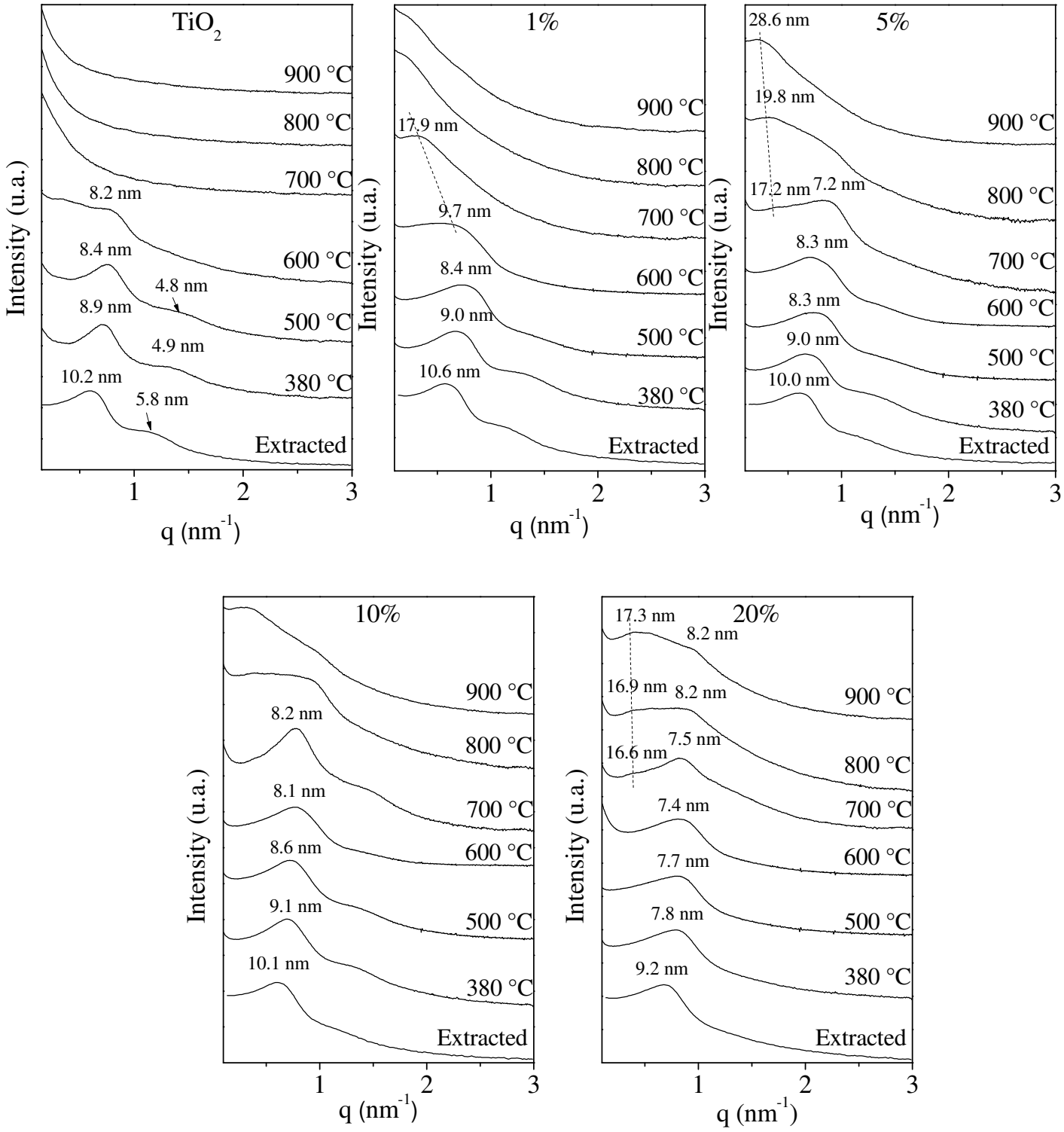
TiO2
900 °C
800 °C
700 °C
8.2 nm
600 °C
8.4 nm
4.8 nm
8.9 nm
500 °C
4.9 nm
10.2 nm
380 °C
5.8 nm
Extracted
Intensity (u.a.)
q (nm-1)
1%
17.9 nm
9.7 nm
8.4 nm
9.0 nm
10.6 nm
5%
28.6 nm
19.8 nm
17.2 nm
7.2 nm
8.3 nm
8.3 nm
9.0 nm
10.0 nm
10%
8.2 nm
8.1 nm
8.6 nm
9.1 nm
10.1 nm
20%
17.3 nm
8.2 nm
16.9 nm
8.2 nm
16.6 nm
7.5 nm
7.4 nm
7.7 nm
7.8 nm
9.2 nm

Figure 2

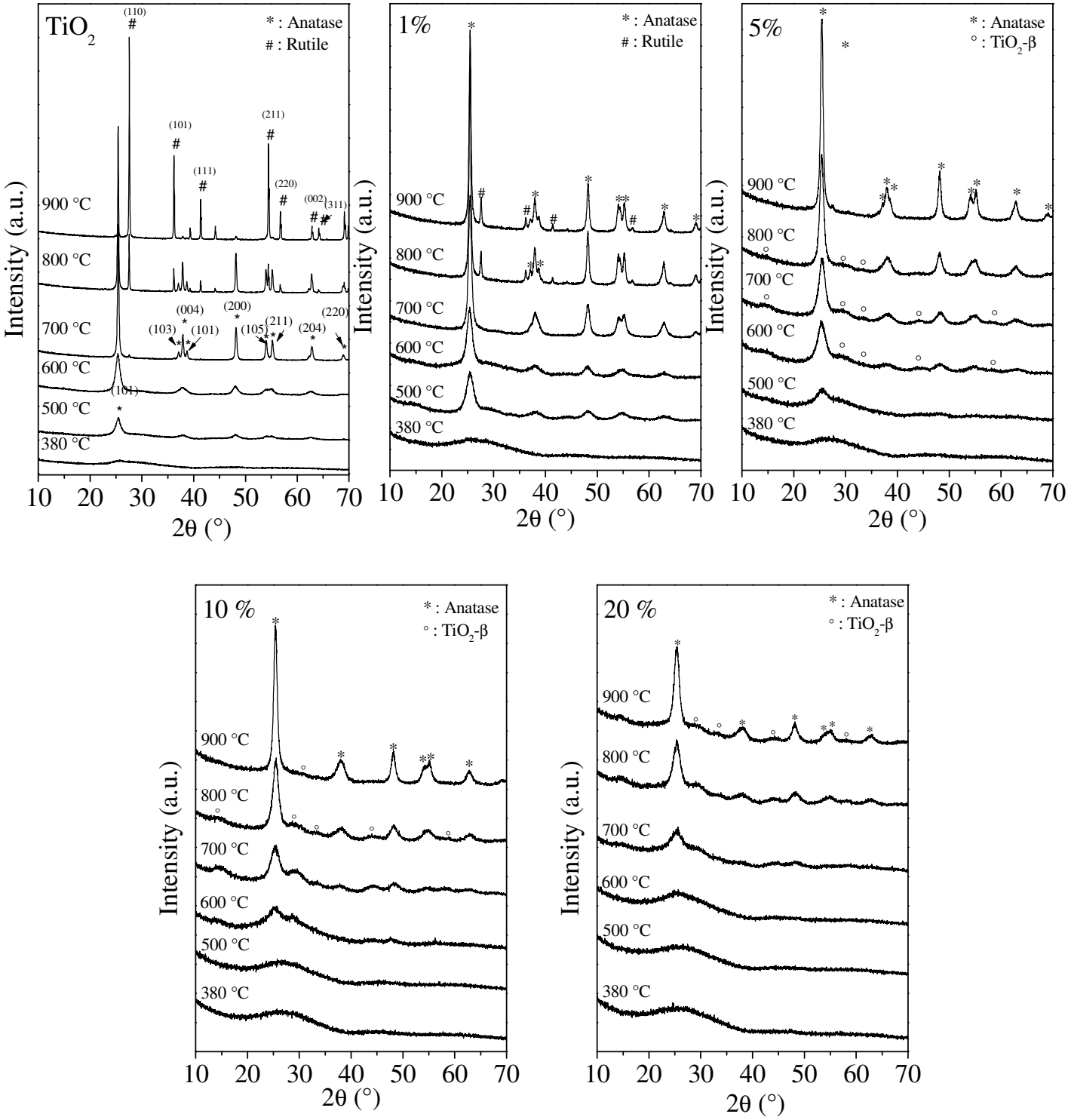
TiO2
* : Anatase
# : Rutile
1%
5%
° : TiO2-β
10 %
20 %
900 °C
800 °C
700 °C
600 °C
500 °C
380 °C
Intensity (a.u.)
2θ (°)

Figure 3

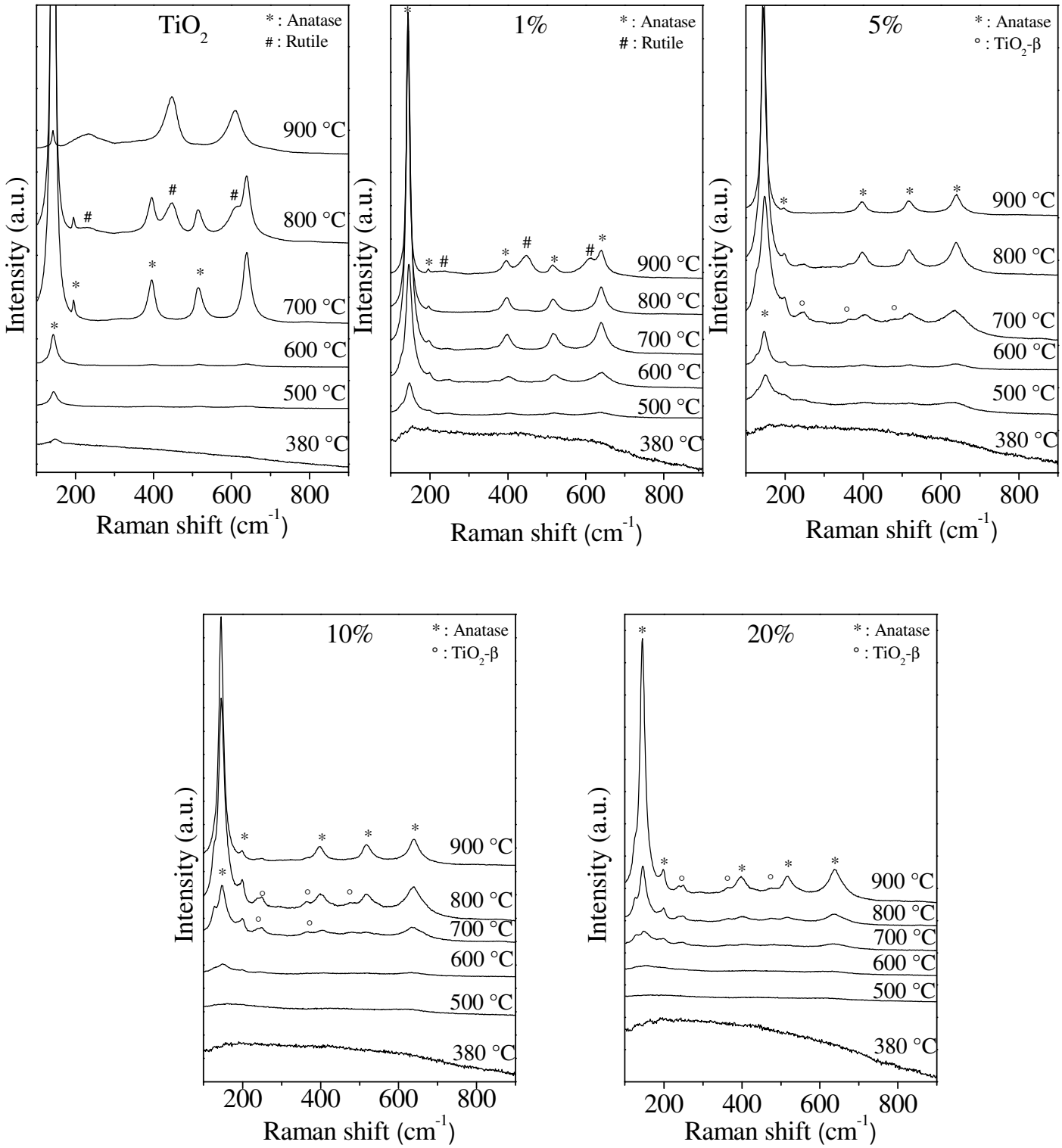
TiO2
* : Anatase
# : Rutile
1%
5%
° : TiO2-β
10%
20%
900 °C
800 °C
700 °C
600 °C
500 °C
380 °C
Intensity (a.u.)
Raman shift (cm-1)
200
400
600
800

Figure 4

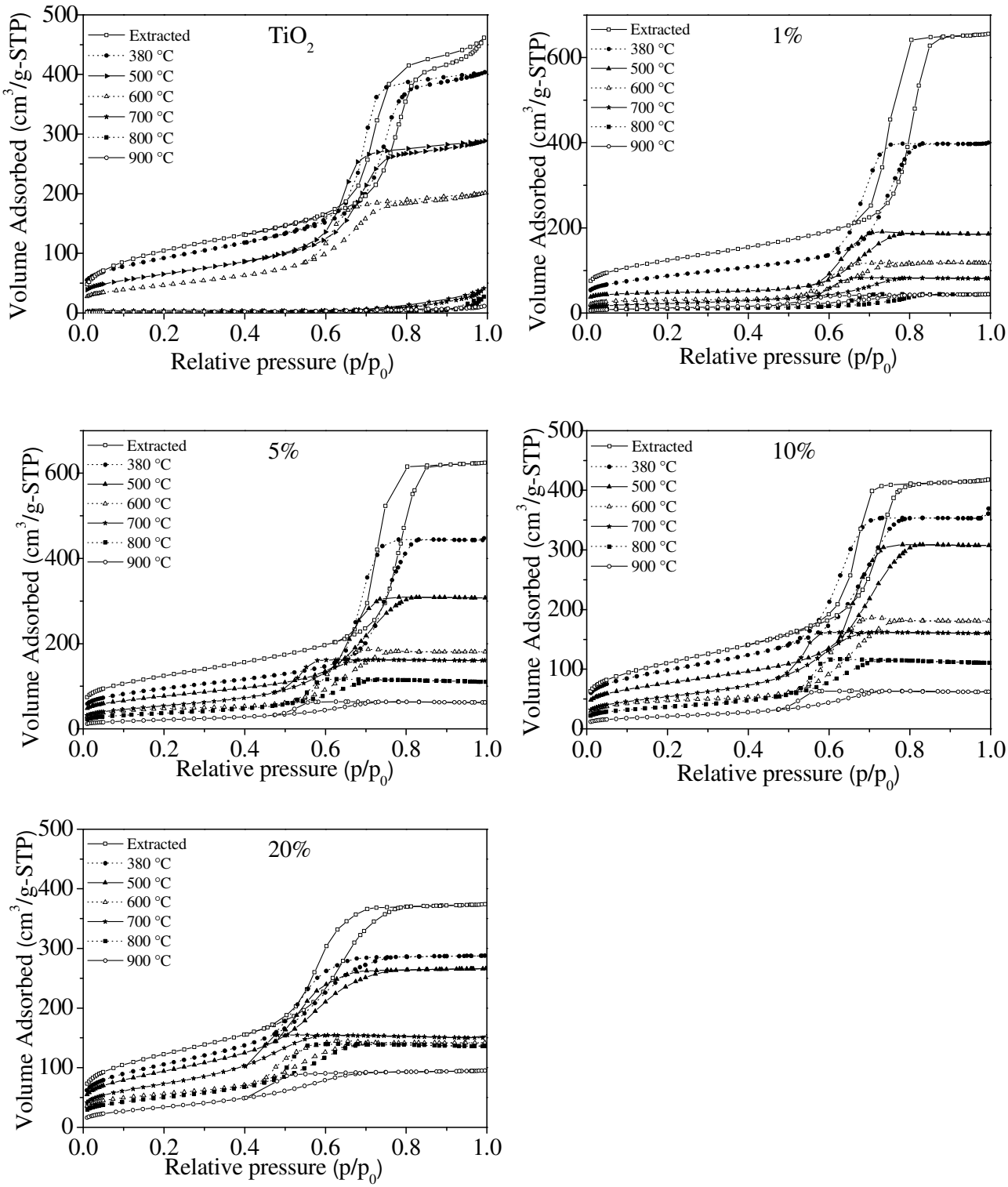
TiO2
1%
5%
10%
20%
Extracted
380 °C
500 °C
600 °C
700 °C
800 °C
900 °C
Volume Adsorbed (cm3/g-STP)
Relative pressure (p/p0)

Figure 5

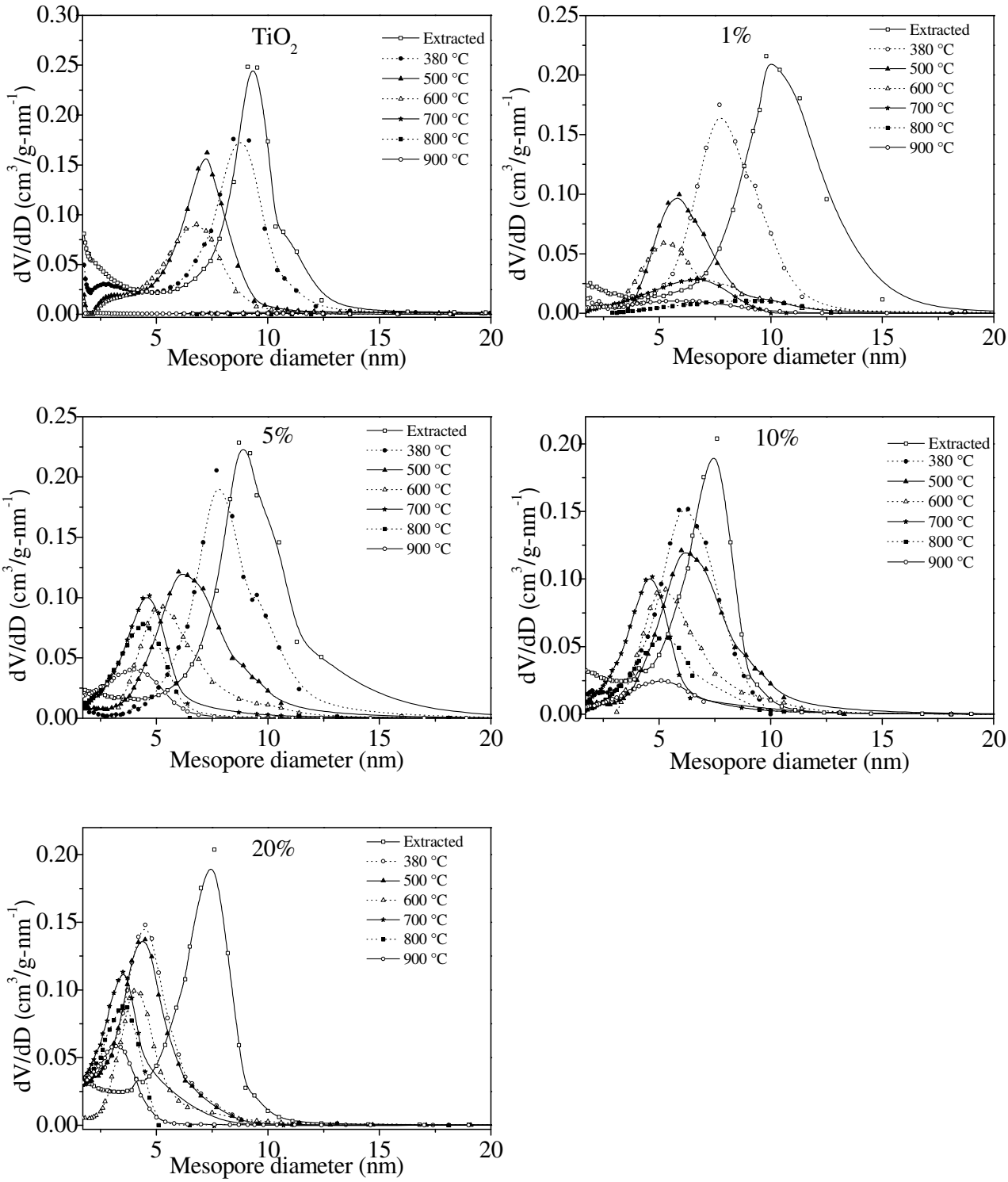
TiO2
1%
5%
10%
20%
Extracted
380 °C
500 °C
600 °C
700 °C
800 °C
900 °C
dV/dD (cm3/g-nm-1)
Mesopore diameter (nm)

Figure 6

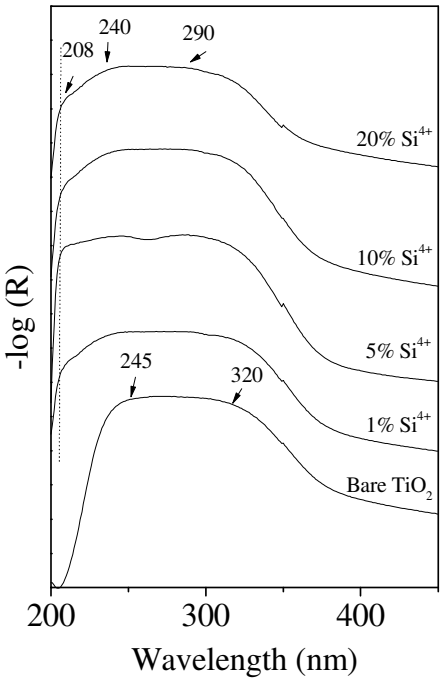
240
208
290
20% Si4+
10% Si4+
5% Si4+
245
320
1% Si4+
Bare TiO2
-log (R)
200
300
400
Wavelength (nm)

Figure 7

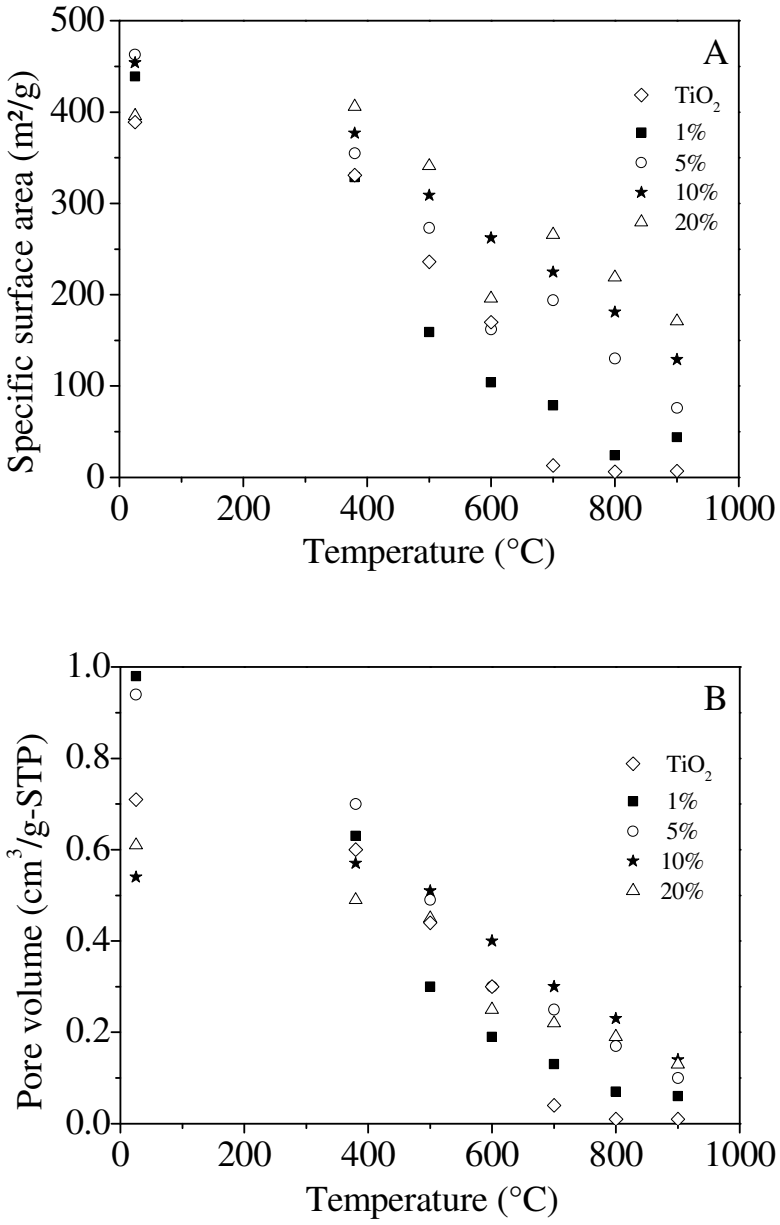
A
Specific surface area (m²/g)
Temperature (°C)
TiO2
1%
5%
10%
20%
B
Pore volume (cm3/g-STP)
Temperature (°C)
TiO2
1%
5%
10%
20%

Figure 8

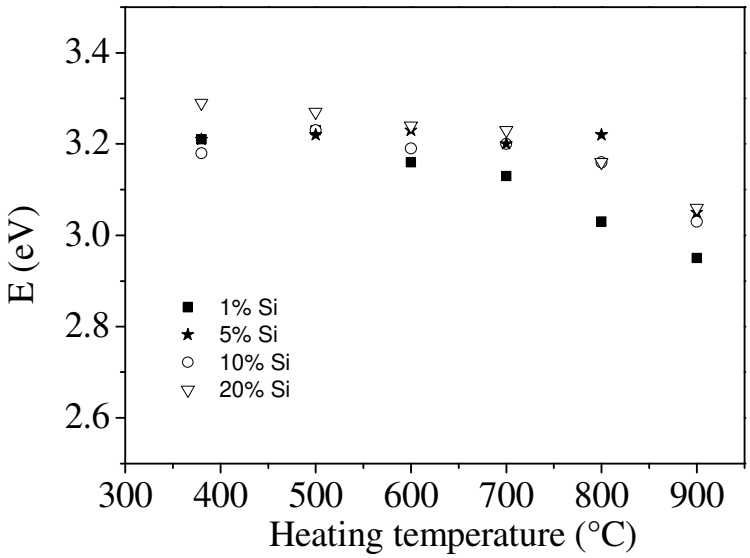
3.4
3.2
3.0
2.8
2.6
E (eV)
1% Si
5% Si
10% Si
20% Si
300
400
500
600
700
800
900
Heating temperature (°C)

Figure 9

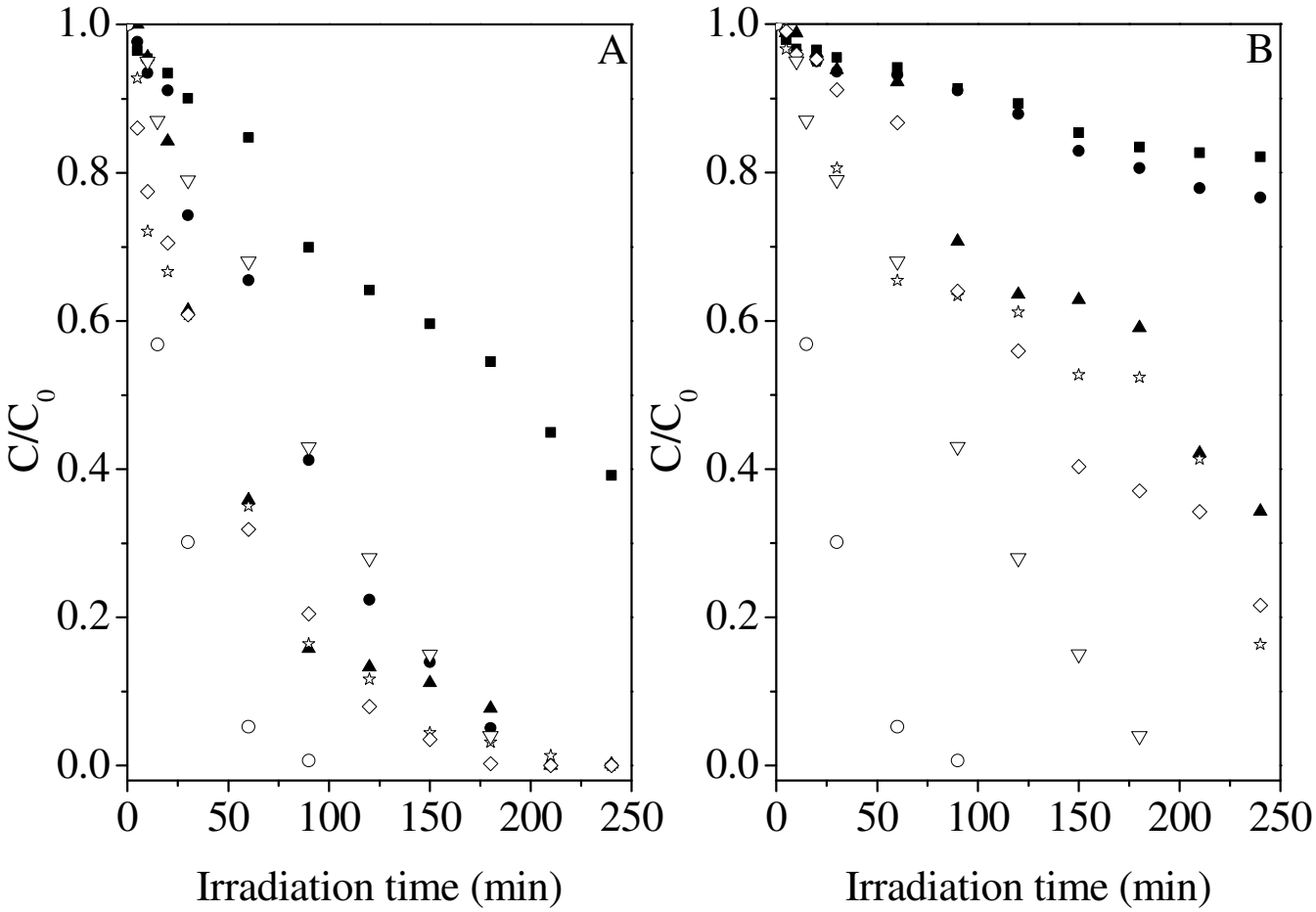
A
B
C/C0
Irradiation time (min)
0.0
0.2
0.4
0.6
0.8
1.0
0
50
100
150
200
250

Figure 10

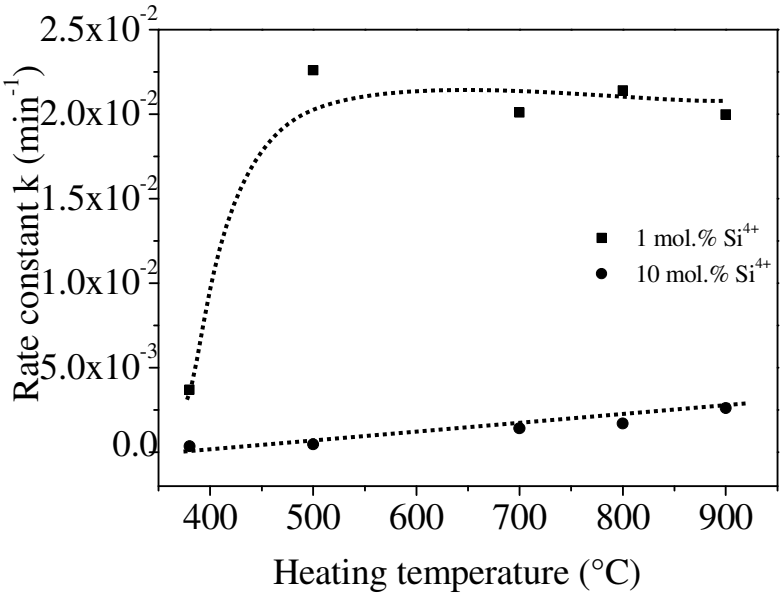
2.5x10-2
2.0x10-2
1.5x10-2
1.0x10-2
5.0x10-3
0.0
Rate constant k (min-1)
1 mol.% Si4+
10 mol.% Si4+
400
500
600
700
800
900
Heating temperature (°C)